

Bi-fidelity conditional value-at-risk estimation by dimensionally decomposed generalized polynomial chaos expansion

Dongjin Lee^{a,*}, Boris Kramer^{a,*}

^a*Department of Mechanical and Aerospace Engineering, University of California San Diego, CA, United States*

January 5, 2023

Abstract

Digital twin models allow us to continuously assess the possible risk of damage and failure of a complex system. Yet high-fidelity digital twin models can be computationally expensive, making quick-turnaround assessment challenging. Towards this goal, this article proposes a novel bi-fidelity method for estimating the conditional value-at-risk (CVaR) for nonlinear systems subject to dependent and high-dimensional inputs. For models that can be evaluated fast, a method that integrates the dimensionally decomposed generalized polynomial chaos expansion (DD-GPCE) approximation with a standard sampling-based CVaR estimation is proposed. For expensive-to-evaluate models, a new bi-fidelity method is proposed that couples the DD-GPCE with a Fourier-polynomial expansion of the mapping between the stochastic low-fidelity and high-fidelity output data to ensure computational efficiency. The method employs measure-consistent orthonormal polynomials in the random variable of the low-fidelity output to approximate the high-fidelity output. Numerical results for a structural mechanics truss with 36-dimensional (dependent random variable) inputs indicate that the DD-GPCE method provides very accurate CVaR estimates that require much lower computational effort than standard GPCE approximations. A second example considers the realistic problem of estimating the risk of damage to a fiber-reinforced composite laminate. The high-fidelity model is a finite element simulation that is prohibitively expensive for risk analysis, such as CVaR computation. Here, the novel bi-fidelity method can accurately estimate CVaR as it includes low-fidelity models in the estimation procedure and uses only a few high-fidelity model evaluations to significantly increase accuracy.

Keywords: Risk measures, conditional value-at-risk, generalized polynomial chaos expansion, dimensionally decomposed GPCE, bi-fidelity modeling

1. Introduction

Risk assessment is essential for designing and maintaining high-performance engineering systems from the conceptual design stage to operation—where digital twins play a growing role—to product retirement. Measures of risk (rather than reliability) have been employed in finance for quite some time, see [1, 41, 43]. For example, the Value-at-Risk (VaR) is based on a quantile of the distribution of the output quantity of interest to measure aggregate losses, while the Conditional Value-at-Risk (CVaR) reflects the mean or average size of losses exceeding the VaR. For optimization in either portfolio management [40, 41, 25] or engineering design [49, 42], CVaR is superior to VaR in that it quantifies tail risk and, as a coherent risk measure, is subadditive [43]. Moreover, in contrast to VaR, CVaR preserves convexity of the function it is applied to, which facilitates optimization [40, 17, 8, 4]. Despite offering convexity, a drawback of CVaR is that it is non-smooth, yet smoothed approximations exist [17, 18], which significantly improve optimization performance. It has also been noted that CVaR has several quantitative and qualitative advantages over reliability (or failure probability), a commonly

*Corresponding author

Email addresses: dongjin-lee@ucsd.edu (Dongjin Lee), bmramer@ucsd.edu (Boris Kramer)

used concept in engineering practice, see [39, 4] for a detailed discussion. Applications of CVaR in the engineering domains, such as the design of civil [39], naval [42], and aerospace [49, 42, 5] engineering, have appeared. Moreover, recent studies imply that CVaR can improve risk management for digital twins [19, 29, 3], encompassing design, procurement, testing, and production.

Since CVaR is a statistical risk measure, its estimation (besides simple cases where an output follows a distribution from a specific parametric family [31]) is mostly performed via a sampling method, such as Monte Carlo Simulation (MCS). The CVaR and other risk measures are typically associated with a tail of the output distribution. Consequently, a large amount of (at least thousands of) output samples should be obtained to capture the tail risk. However, in most engineering systems, the output (or response) of a system can only be obtained through experiments or computer simulation. The latter is most commonly done through finite element analysis (FEA) or other spatial discretization techniques which can require high computational cost. This makes CVaR estimation computationally intensive if not prohibitive when crude MCS is employed. This situation is compounded when CVaR is used within an optimization problem. To mitigate some of these computational challenges, numerous surrogate methods coupled with other variance reduction techniques for CVaR estimation have been developed, such as reduced-order models (ROMs) [12, 50, 11], polynomial chaos expansion (PCE) [2], Kriging [6], support vector machine [9], and neural networks [45]. In addition, recent work [15] presents a surrogate modeling method to train the PCE or other surrogate models using limited samples for conservatively estimating CVaR. The method constructs a surrogate model that is tailored to the user’s risk preferences (biased to risk measure) while allowing for overestimating risk. That work, and most existing other methods, make the simplifying assumption that the input random variables are statistically independent, which then allows factoring their joint probability distribution as the tensor product of the marginal probability distributions of the input variables. However, in practice, input variables are often correlated or dependent. Indeed, neglecting the correlation in input random variables, whether emanating from loads, material properties, or manufacturing variables may produce inaccurate or unknown risky designs [30, 21].

Standard MCS can be used to sample directly from dependent random variables, yet MCS requires only high-fidelity model evaluations and therefore can be computationally prohibitive. A few other estimation methods, such as generalized PCE (GPCE) [37], generalized polynomial dimensional decomposition (GPDD) [38], or other PCE variants [28, 14], can handle dependent random variables directly without a potentially detrimental measure transformation between dependent and independent variables. A practical version of the GPCE was recently introduced to effectively solve UQ and design optimization problems under arbitrary, dependent input random variables [21, 22, 23]. This work makes it possible to obtain the multivariate orthonormal polynomial basis consistent with any non-product-type probability measure of input numerically, instead of an analytical expression by a Rodrigues-type formula used in the prequel [37]. Most recently, a dimensionally decomposed GPCE (DD-GPCE) [20] has been introduced to tackle stochastic design problems with high-dimensional inputs. As a restructured version of GPCE, the DD-GPCE has been proven to alleviate the curse of dimensionality to some extent by reshuffling and pruning GPCE basis functions in a dimension-wise manner. Two current shortcomings of the DD-GPCE are that, first, the DD-GPCE method has been evaluated only for statistical moment and reliability analyses in design problems. Yet, as elaborated above, in engineering design, risk measures such as CVaR are an interesting alternative and often superior. Second, the DD-GPCE often mandates hundreds of high-fidelity model evaluations which can be computationally prohibitive depending on the complexity and state dimension of the computational models (often FEA models).

This study therefore focuses on CVaR estimation of nonlinear and high-dimensional systems under dependent random variables and enables scalability both with respect to the high state dimension and the high input parameter dimension. Specifically, we propose a novel bi-fidelity method for CVaR estimation of nonlinear systems with high-dimensional, correlated input random variables and/or nonlinear responses. The novel method combines (1) the DD-GPCE approximation of a high-dimensional stochastic output function, (2) an innovative method using Fourier-polynomial expansions of the map-

ping between the stochastic low-fidelity and high-fidelity output data for efficiently calculating the DD-GPCE, and (3) a standard sampling-based CVaR estimation integrated with the DD-GPCE. In contrast to existing bi- or multi-fidelity methods based on an additive and/or multiplicative correction to the low fidelity output [16, 34, 33], the proposed bi-fidelity method employs linear or higher-order orthonormal basis functions consistent with the probability measure of the low-fidelity output to approximate the high-fidelity output, thus achieving nearly exponential convergence rate for the output data. Such Fourier-polynomial approximations demand only a handful of high-fidelity output evaluations. The lower-fidelity outputs are determined by DD-GPCE approximations to reduce the computational costs further.

The paper is organized as follows. Section 2 discusses mathematical notations and preliminaries, including input and output random variables and alternative expressions of CVaR. Also, brief explanations of the GPCE and DD-GPCE methods are provided. Section 3 presents a sampling-based CVaR estimation by the DD-GPCE method. Section 4 introduces a novel bi-fidelity method for precise and computationally efficient CVaR estimation that requires only a few expensive high-fidelity model evaluations. Numerical results are reported in Section 5. Finally, the conclusions are drawn and future directions outlines in Section 6.

2. Background and related methods

This section presents our problem setup and definitions in Section 2.1, discusses alternative CVaR definitions in Section 2.2 and briefly summarizes the GPCE in Section 2.3 and the DD-GPCE in Section 2.4.

2.1. Problem setup and definitions

Let \mathbb{N} , \mathbb{N}_0 , \mathbb{R} , and \mathbb{R}_0^+ be the sets of positive integers, non-negative integers, real numbers, and non-negative real numbers, respectively. For a positive integer $N \in \mathbb{N}$, denote by $\mathbb{A}^N \subseteq \mathbb{R}^N$ a bounded or unbounded sub-domain of \mathbb{R}^N .

2.1.1. Input random variables

Let $(\Omega, \mathcal{F}, \mathbb{P})$ be a probability triple, where Ω is a sample space representing an abstract set of elementary events, \mathcal{F} is a σ -algebra on Ω , and $\mathbb{P} : \mathcal{F} \rightarrow [0, 1]$ is a probability measure. Then, consider an N -dimensional random vector $\mathbf{X} := (X_1, \dots, X_N)^\top$, describing the statistical uncertainties in all input and system parameters of a stochastic or random problem. Every so often, \mathbf{X} will be referred to as an input random vector or input random variables where the integer N represents the total number of input random variables.

Denote by $F_{\mathbf{X}}(\mathbf{x}) := \mathbb{P}[\cap_{i=1}^N \{X_i \leq x_i\}]$ the joint distribution function of \mathbf{X} , admitting the joint probability density function $f_{\mathbf{X}}(\mathbf{x}) := \partial^N F_{\mathbf{X}}(\mathbf{x}) / \partial x_1 \cdots \partial x_N$. Given the abstract probability space $(\Omega, \mathcal{F}, \mathbb{P})$, the image probability space is $(\mathbb{A}^N, \mathcal{B}^N, f_{\mathbf{X}} d\mathbf{x})$, where \mathbb{A}^N can be viewed as the image of Ω from the mapping $\mathbf{X} : \Omega \rightarrow \mathbb{A}^N$ and $\mathcal{B}^N := \mathcal{B}(\mathbb{A}^N)$ is the Borel σ -algebra on $\mathbb{A}^N \subset \mathbb{R}^N$.

We make the following assumptions, which are identical to [37].

Assumption 1. *The random vector $\mathbf{X} := (X_1, \dots, X_N)^\top$*

1. *has an absolutely continuous joint distribution function $F_{\mathbf{X}}(\mathbf{x})$ and a continuous joint probability density function $f_{\mathbf{X}}(\mathbf{x})$ with a bounded or unbounded support $\mathbb{A}^N \subseteq \mathbb{R}^N$;*
2. *possesses absolute finite moments of all orders, that is, for all $\mathbf{j} := (j_1, \dots, j_N) \in \mathbb{N}_0^N$, it holds that*

$$\mathbb{E}[|\mathbf{X}^{\mathbf{j}}|] := \int_{\Omega} |\mathbf{X}(\omega)|^{\mathbf{j}} d\mathbb{P}(\omega) = \int_{\mathbb{A}^N} |\mathbf{x}^{\mathbf{j}}| f_{\mathbf{X}}(\mathbf{x}) d\mathbf{x} < \infty, \quad (1)$$

where $\mathbf{X}^{\mathbf{j}} = X_1^{j_1} \cdots X_N^{j_N}$ and \mathbb{E} is the expectation operator with respect to the probability measure \mathbb{P} or $f_{\mathbf{X}}(\mathbf{x}) d\mathbf{x}$;

3. has a joint probability density function $f_{\mathbf{X}}(\mathbf{x})$, which

- (a) has a compact support, that is, there exists a compact subset $\mathbb{A}^N \subset \mathbb{R}^N$ such that $\mathbb{P}[\mathbf{X} \in \mathbb{A}^N] = 1$, or
- (b) is exponentially integrable, that is, there exists a real number $\alpha > 0$ such that

$$\int_{\mathbb{A}^N} \exp(\alpha \|\mathbf{x}\|) f_{\mathbf{X}}(\mathbf{x}) d\mathbf{x} < \infty, \quad (2)$$

where $\|\cdot\| : \mathbb{A}^N \rightarrow \mathbb{R}_0^+$ is an arbitrary norm.

2.1.2. Output random variable

Given an input random vector $\mathbf{X} := (X_1, \dots, X_N)^\top : \Omega \rightarrow \mathbb{A}^N$ with a known probability density function $f_{\mathbf{X}}(\mathbf{x})$ on $\mathbb{A}^N \subseteq \mathbb{R}^N$, denote by $y(\mathbf{X}) := y(X_1, \dots, X_N)$ a real-valued, square-integrable output random variable. Here, $y : \mathbb{A}^N \rightarrow \mathbb{R}$ describes a quantity of interest that an application engineer deems relevant for risk assessment. In this work, y is assumed to belong to the weighted L^2 space

$$\left\{ y : \mathbb{A}^N \rightarrow \mathbb{R} : \int_{\mathbb{A}^N} |y(\mathbf{x})|^2 f_{\mathbf{X}}(\mathbf{x}) d\mathbf{x} < \infty \right\},$$

which is a Hilbert space. This is tantamount to saying that, for the abstract probability space $(\Omega, \mathcal{F}, \mathbb{P})$, the output random variable $Y = y(\mathbf{X})$ belongs to the equivalent Hilbert space

$$L^2(\Omega, \mathcal{F}, \mathbb{P}) := \left\{ Y : \Omega \rightarrow \mathbb{R} : \int_{\Omega} |y(\mathbf{X}(\omega))|^2 d\mathbb{P}(\omega) < \infty \right\}.$$

If there is more than one output variable, then each component is associated with a measurement function y_i . Indeed, the generalization for a multivariate output random vector is straightforward.

2.2. Conditional Value-at-Risk

Given a random input $\mathbf{X} = (X_1, \dots, X_N)^\top$, consider an output function $y(\mathbf{X}) \in L^2(\Omega, \mathcal{F}, \mathbb{P})$. For a given risk level $\beta \in (0, 1)$, denote by $\text{CVaR}_\beta[y(\mathbf{X})]$ and $\text{VaR}_\beta[y(\mathbf{X})]$ the conditional value-at-risk and the value-at-risk of $y(\mathbf{X})$ at level β , respectively. The $\text{VaR}_\beta[y(\mathbf{X})]$ is the β -quantile of $y(\mathbf{X})$, i.e.,

$$\text{VaR}_\beta[y(\mathbf{X})] = \arg \min_{t \in \mathbb{R}} \{\mathbb{P}[y(\mathbf{X}) \leq t] \geq \beta\}, \quad (3)$$

where $\mathbb{P}[y(\mathbf{X}) \leq t] = \int_{\mathbb{A}^N} \mathbb{I}_{\{y(\mathbf{x}) \leq t\}}(\mathbf{x}) f_{\mathbf{X}}(\mathbf{x}) d\mathbf{x}$. Here, the indicator function is

$$\mathbb{I}_{\{y(\mathbf{x}) \leq t\}}(\mathbf{x}) = \begin{cases} 1, & y(\mathbf{x}) \leq t, \\ 0, & \text{otherwise.} \end{cases}$$

The $\text{CVaR}_\beta[y(\mathbf{X})]$ is predicated on the mean value of $y(\mathbf{X})$ exceeding $\text{VaR}_\beta[y(\mathbf{X})]$. There exist several different equivalent definitions of CVaR_β . Following [40, 41], the CVaR_β at level $\beta \in (0, 1)$ is

$$\text{CVaR}_\beta[y(\mathbf{X})] = \arg \min_{t \in \mathbb{R}} \left\{ t + \frac{1}{1 - \beta} \mathbb{E}[(y(\mathbf{X}) - t)_+] \right\}, \quad (4)$$

where $(\cdot)_+ = \max(\cdot, 0)$ and \mathbb{E} is the expectation with respect to $f_{\mathbf{X}}(\mathbf{x}) d\mathbf{x}$. The minimum of (4) on the interval $\text{VaR}_\beta[y(\mathbf{X})] \leq t \leq \sup \{t : \mathbb{P}[y(\mathbf{X}) \leq t] \leq \beta\}$ is determined by inserting $\text{VaR}_\beta[y(\mathbf{X})]$ into (4), that is,

$$\text{CVaR}_\beta[y(\mathbf{X})] = \text{VaR}_\beta[y(\mathbf{X})] + \frac{1}{1 - \beta} \mathbb{E}[(y(\mathbf{X}) - \text{VaR}_\beta[y(\mathbf{X})])_+]. \quad (5)$$

If the cumulative distribution function (CDF) $\mathbb{P}[Y \leq y]$ is continuous at $y = \text{VaR}_\beta[y(\mathbf{X})]$, the equation (5) can be simplified, i.e.,

$$\text{CVaR}_\beta[y(\mathbf{X})] = \frac{1}{1-\beta} \mathbb{E}[y(\mathbf{X}) \cdot \mathbb{I}_{\{y(\mathbf{X}) \geq \text{VaR}_\beta[y(\mathbf{X})]\}}(\mathbf{X})]. \quad (6)$$

Having the definition of CVaR and the relevant definitions at hand, we can now formally state the problem that is considered in this paper.

Problem 1. Consider a high-dimensional dependent random input vector $\mathbf{X} \in \mathbb{A}^N$ following an arbitrary probability measure $f_{\mathbf{X}}(\mathbf{x})d\mathbf{x}$, and that satisfies Assumption 1. Moreover, we are given an expensive-to-evaluate output quantity of interest $y : \mathbb{A}^N \mapsto \mathbb{R}$. The goal is to compute the $\text{CVaR}_\beta[y(\mathbf{X})]$ efficiently.

2.3. Generalized polynomial chaos expansion

A generalized PCE (GPCE) of a square-integrable random variable $y(\mathbf{X})$ is the expansion of $y(\mathbf{X})$ in terms of an orthonormal polynomial basis in the input variables \mathbf{X} . We briefly review GPCE in this section. When $\mathbf{X} = (X_1, \dots, X_N)^\top$ comprises statistically dependent random variables, the resultant probability measure, in general, is not a product-type, meaning that the joint distribution of \mathbf{X} cannot be obtained strictly from its marginal distributions. Consequently, measure-consistent multivariate orthonormal polynomials in $\mathbf{x} = (x_1, \dots, x_N)^\top$ cannot be built from an N -dimensional tensor product of measure-consistent univariate orthonormal polynomials. In this case, a three-step algorithm based on a whitening transformation of the monomial basis can be used to determine multivariate orthonormal polynomials consistent with an arbitrary, non-product-type probability measure $f_{\mathbf{X}}(\mathbf{x})d\mathbf{x}$ of \mathbf{X} , which will be exploited in the Section 2.4.1 and Appendix A.

Let $\mathbf{j} := (j_1, \dots, j_N) \in \mathbb{N}_0^N$ be an N -dimensional multi-index. For a realization $\mathbf{x} = (x_1, \dots, x_N)^\top \in \mathbb{A}^N \subseteq \mathbb{R}^N$ of \mathbf{X} , a monomial in the real variables x_1, \dots, x_N is the product $\mathbf{x}^{\mathbf{j}} = x_1^{j_1} \dots x_N^{j_N}$ with a total degree $|\mathbf{j}| = j_1 + \dots + j_N$. Consider for each $m \in \mathbb{N}_0$ the elements of the multi-index set

$$\mathcal{J}_m := \{\mathbf{j} \in \mathbb{N}_0^N : |\mathbf{j}| \leq m\},$$

which is arranged as $\mathbf{j}^{(1)}, \dots, \mathbf{j}^{(L_{N,m})}$, $\mathbf{j}^{(1)} = \mathbf{0}$, according to a monomial order of choice. The set \mathcal{J}_m has cardinality $L_{N,m}$ obtained as

$$L_{N,m} := |\mathcal{J}_m| = \sum_{l=0}^m \binom{N+l-1}{l} = \binom{N+m}{m}. \quad (7)$$

Let us denote by

$$\boldsymbol{\Psi}_m(\mathbf{x}) = (\Psi_1(\mathbf{x}), \dots, \Psi_{L_{N,m}}(\mathbf{x}))^\top \quad (8)$$

an $L_{N,m}$ -dimensional vector of multivariate orthonormal polynomials that are consistent with the probability measure $f_{\mathbf{X}}(\mathbf{x})d\mathbf{x}$ of \mathbf{X} . Consequently, any output random variable $y(\mathbf{X}) \in L^2(\Omega, \mathcal{F}, \mathbb{P})$ can be approximated by the m th-order GPCE¹

$$y_m(\mathbf{X}) = \sum_{i=1}^{L_{N,m}} c_i \Psi_i(\mathbf{X}) \quad (9)$$

¹The GPCE in (9) should not be confused with that of [48]. The GPCE, presented here, is meant for an arbitrary dependent probability distribution of random input. In contrast, the existing PCE, whether classical [47] or generalized [48], still requires independent random inputs.

of $y(\mathbf{X})$, comprising $L_{N,m}$ basis functions with expansion coefficients

$$c_i := \int_{\mathbb{A}^N} y(\mathbf{x}) \Psi_i(\mathbf{x}) f_{\mathbf{X}}(\mathbf{x}) d\mathbf{x}, i = 1, \dots, L_{N,m}. \quad (10)$$

Here, the orthonormal polynomials $\Psi_i(\mathbf{X})$, $i = 1, \dots, L_{N,m}$, are determined by the three steps in [Appendix A](#). We refer to [21] for more details. The GPCE is referred to as regular GPCE to distinguish it from the DD-GPCE which is introduced next.

2.4. Dimensionally decomposed generalized polynomial chaos expansion

For problems with high-dimensional inputs (say, $N \geq 20$), the regular GPCE approximation in (9) requires a relatively large number of basis functions due to the growth of $L_{N,m}$ in (7), which reflects the curse of dimensionality. For example, for a total degree of $m = 3$, consider an increase of N from 20 to 50. The respective number of the regular GPCE's basis functions exponentially increases from 1,771 to 23,426. However, in many real-world applications, high-variate interaction effects among input variables are often negligible to the output function value of interest [35, 36]. In such cases, we can leverage the DD-GPCE method to reorder the basis functions of the regular GPCE in a dimension-wise manner that then allows for effectively truncating them to tackle high-dimensional problems. In the next section, the DD-GPCE is briefly summarized, see [20] for details.

2.4.1. Measure-consistent orthonormal polynomials

The DD-GPCE has the ability to effectively select a subset of the basis functions of the regular GPCE based on the degree of interaction among input variables. Consequently, the method can capture complex nonlinear behavior of the output functions while reducing the exponential growth of the basis functions. The chosen multivariate orthonormal polynomials that are consistent with an arbitrary, non-product-type probability measure $f_{\mathbf{X}}(\mathbf{x})d\mathbf{x}$ of \mathbf{x} are determined by the three-step process based on a whitening transformation of the monomial basis as follows.

For $N \in \mathbb{N}$, denote by $\{1, \dots, N\}$ an index set and $\mathcal{U} \subseteq \{1, \dots, N\}$ a subset (including the empty set \emptyset) with cardinality $0 \leq |\mathcal{U}| \leq N$. The complementary subset of \mathcal{U} is denoted by $\mathcal{U}^c := \{1, \dots, N\} \setminus \mathcal{U}$. For each $m \in \mathbb{N}_0$ and $0 \leq S \leq N$, we define the reduced multi-index set

$$\mathcal{J}_{S,m} := \{\mathbf{j} = (\mathbf{j}_{\mathcal{U}}, \mathbf{0}_{\mathcal{U}^c}) \in \mathbb{N}_0^N : \mathbf{j}_{\mathcal{U}} \in \mathbb{N}^{|\mathcal{U}|}, |\mathcal{U}| \leq |\mathbf{j}_{\mathcal{U}}| \leq m, 0 \leq |\mathcal{U}| \leq S\}, \quad (11)$$

which is arranged as $\mathbf{j}^{(1)}, \dots, \mathbf{j}^{(L_{N,S,m})}$, $\mathbf{j}^{(1)} = \mathbf{0}$, according to a monomial order of choice and where $|\mathbf{j}_{\mathcal{U}}| := j_{i_1} + \dots + j_{i_{|\mathcal{U}|}}$. Here, $(\mathbf{j}_{\mathcal{U}}, \mathbf{0}_{\mathcal{U}^c})$ denotes an N -dimensional multi-index whose i th component is j_i if $i \in \mathcal{U}$ and 0 if $i \notin \mathcal{U}$. It is straightforward to show that $\mathcal{J}_{S,m}$ has cardinality

$$L_{N,S,m} := |\mathcal{J}_{S,m}| = 1 + \sum_{s=1}^S \binom{N}{s} \binom{m}{s}. \quad (12)$$

The set $\mathcal{J}_{S,m}$ represents a subset of \mathcal{J}_m determined from the chosen S , where only at most S -variate basis functions are preserved, that are relevant for the S th-variate DD-GPCE approximation. For example, univariate ($S = 1$) and bivariate ($S = 2$) DD-GPCE approximations demand $Nm + 1$ and $N(N - 1)m(m - 1)/4 + Nm + 1$ basis functions, respectively, according to (12). The expression “ S -variate” used for the DD-GPCE approximation means that at most S -degree interaction of input variables are included. As an example, univariate and bivariate input variables are x_i and $x_{i_1}x_{i_2}$, where $i_1 \neq i_2$, respectively. Thus, the DD-GPCE approximation, the sum of at most S -variate basis functions, is strictly an N -variate function, which will be explained in detail in the following subsection. As a result, we have that

$$L_{N,S,m} \leq L_{N,m},$$

i.e., the DD-GPCE never has more terms than the standard GPCE; in most cases, it will have significantly less terms. For $\mathbf{x} = (x_1, \dots, x_N)^\top \in \mathbb{A}^N \subseteq \mathbb{R}^N$ we then define the basis vector for the

DD-GPCE as

$$\Psi_{S,m}(\mathbf{x}) := (\Psi_1(\mathbf{x}), \dots, \Psi_{L_{N,S,m}}(\mathbf{x}))^\top,$$

which is an $L_{N,S,m}$ -dimensional vector of multivariate orthonormal polynomials that is consistent with the probability measure $f_{\mathbf{X}}(\mathbf{x})d\mathbf{x}$ of \mathbf{x} . The orthonormal polynomials are determined by the following three steps.

Step 1. Given $0 \leq S \leq N$ and $S \leq m < \infty$, create an $L_{N,S,m}$ -dimensional column vector

$$\mathbf{M}_{S,m}(\mathbf{x}) = (\mathbf{x}^{\mathbf{j}^{(1)}}, \dots, \mathbf{x}^{\mathbf{j}^{(L_{N,S,m})}})^\top \quad (13)$$

of monomials whose elements are the monomials $\mathbf{x}^{\mathbf{j}}$ for $\mathbf{j} \in \mathcal{J}_{S,m}$ arranged in the aforementioned order. For $\mathcal{U} \subseteq \{1, \dots, N\}$, let $\mathbf{x}_{\mathcal{U}} := (x_{i_1}, \dots, x_{i_{|\mathcal{U}|}})^\top$, $1 \leq i_1 < \dots < i_{|\mathcal{U}|} \leq N$, be a subvector of \mathbf{x} . The complementary subvector is defined by $\mathbf{x}_{\mathcal{U}^c} := \mathbf{x}_{\{1, \dots, N\} \setminus \mathcal{U}}$. Then, for $\mathbf{j} \in \mathcal{J}_{S,m}$,

$$\mathbf{x}^{\mathbf{j}} = \mathbf{x}_{\mathcal{U}}^{\mathbf{j}_{\mathcal{U}}} \mathbf{0}_{\mathcal{U}^c}^{\mathbf{j}_{\mathcal{U}^c}} = \mathbf{x}_{\mathcal{U}}^{\mathbf{j}_{\mathcal{U}}}.$$

Hence, $\mathbf{M}_{S,m}(\mathbf{x})$ is the monomial vector in $\mathbf{x}_{\mathcal{U}} = (x_{i_1}, \dots, x_{i_{|\mathcal{U}|}})^\top$ of degree $0 \leq |\mathcal{U}| \leq S$ and $|\mathcal{U}| \leq |\mathbf{j}_{\mathcal{U}}| \leq m$.

Step 2. Construct an $L_{N,S,m} \times L_{N,S,m}$ monomial moment matrix of $\mathbf{M}_{S,m}(\mathbf{X})$, defined as

$$\mathbf{G}_{S,m} := \mathbb{E}[\mathbf{M}_{S,m}(\mathbf{X})\mathbf{M}_{S,m}^\top(\mathbf{X})] = \int_{\mathbb{A}^N} \mathbf{M}_{S,m}(\mathbf{x})\mathbf{M}_{S,m}^\top(\mathbf{x})f_{\mathbf{X}}(\mathbf{x})d\mathbf{x}. \quad (14)$$

For an arbitrary PDF $f_{\mathbf{X}}(\mathbf{x})$, the matrix $\mathbf{G}_{S,m}$ cannot be determined exactly, yet it can be accurately estimated with numerical integration and/or sampling methods [21].

Step 3. Select the $L_{N,S,m} \times L_{N,S,m}$ whitening matrix $\mathbf{W}_{S,m}$ from the Cholesky decomposition of the monomial moment matrix $\mathbf{G}_{S,m}$ [37], leading to

$$\mathbf{W}_{S,m}^{-1} \mathbf{W}_{S,m}^{-\top} = \mathbf{G}_{S,m}. \quad (15)$$

Then employ the whitening transformation to generate multivariate orthonormal polynomials from

$$\Psi_{S,m}(\mathbf{x}) = \mathbf{W}_{S,m} \mathbf{M}_{S,m}(\mathbf{x}). \quad (16)$$

It is straightforward to show that $\mathbf{G}_{S,m}$ is symmetric and positive definite. However, the effectiveness of the three-step algorithm is dependent on reliable construction of a well-conditioned monomial moment matrix. That is, numerical issues with the Cholesky factorization in (15) can occur if the estimated matrix has a large condition number.

For the i th element $\Psi_i(\mathbf{X})$ of the orthonormal polynomial vector $\Psi_{S,m}(\mathbf{X}) = (\Psi_1(\mathbf{X}), \dots, \Psi_{L_{N,S,m}}(\mathbf{X}))^\top$, the first- and second-order moments are [21]

$$\mathbb{E}[\Psi_i(\mathbf{X})] = \begin{cases} 1, & \text{if } i = 1, \\ 0, & \text{if } i \neq 1, \end{cases} \quad (17)$$

and

$$\mathbb{E}[\Psi_i(\mathbf{X})\Psi_j(\mathbf{X})] = \begin{cases} 1, & i = j, \\ 0, & i \neq j, \end{cases} \quad (18)$$

respectively. These properties are essential to DD-GPCE which we exploit in the next section. Interested readers may consult Section 6.2.1.4 of [20] for an illustrative example of measure-consistent orthonormal polynomials and a comparison between the DD-GPCE and the regular GPCE.

2.4.2. DD-GPCE approximation

The S -variate, m th-order DD-GPCE approximation of $y(\mathbf{X})$ is

$$y_{S,m}(\mathbf{X}) = \sum_{i=1}^{L_{N,S,m}} c_i \Psi_i(\mathbf{X}) \simeq y \quad (19)$$

with expansion coefficients

$$c_i := \int_{\mathbb{A}^N} y(\mathbf{x}) \Psi_i(\mathbf{x}) f_{\mathbf{X}}(\mathbf{x}) d\mathbf{x}, \quad i = 1, \dots, L_{N,S,m}. \quad (20)$$

The truncation parameters S and m should satisfy $1 \leq S \leq N$ and $S \leq m < \infty$. The DD-GPCE approximation has the property that its basis functions retain the degree of interaction among input variables less than or equal to S and preserves polynomial orders less than or equal to m .

Since the regular GPCE of $y(\mathbf{X}) \in L^2(\Omega, \mathcal{F}, \mathbb{P})$ converges as $m \rightarrow \infty$ in the mean-square sense—both in probability and in distribution, see [21, Theorem 1]—the DD-GPCE $y_{S,m}(\mathbf{X})$ converges to $y(\mathbf{X})$ in the same sense as the regular GPCE as $S \rightarrow N$ and $m \rightarrow \infty$. When y itself is a polynomial function, the DD-GPCE with the same degree (S) and same order (m) of y represents y exactly.

2.4.3. Expansion coefficients

The expansion coefficients c_i , $i = 1, \dots, L_{N,S,m}$, of an S -variate, m th-order DD-GPCE approximation $y_{S,m}(\mathbf{X})$ are determined via high-dimensional integration. For an arbitrary function y and an arbitrary probability distribution of the random input \mathbf{X} , evaluating the integrals exactly from the definition is impossible. Thus, we need to integrate numerically; yet numerical integration via, e.g., a multivariate, tensor-product Gauss-type quadrature rule becomes computationally intensive, if not prohibitive, when $N \geq 10$ (say). For example, if an expansion coefficient is estimated by $N = 10$ dimensional numerical integration with a 3-point rule for each variable, the total number of integrand evaluations is $3^{10} = 59,049$. To address this difficulty, standard least-squares (SLS), as briefly outlined next, can be employed to estimate the coefficients.

Given the known distribution of a random input \mathbf{X} and an output function $y : \mathbb{A}^N \rightarrow \mathbb{R}$, consider an input-output data set $\{\mathbf{x}^{(l)}, y(\mathbf{x}^{(l)})\}_{l=1}^{L'}$ of size $L' \in \mathbb{N}$ generated by evaluating the quantity of interest y at each input data $\mathbf{x}^{(l)}$. Various sampling methods such as standard MCS, Quasi-MCS (QMCS), and Latin hypercube sampling (LHS) or various optimal design of experiments can be employed to build the data set such that the observed distribution underlying the data is consistent with the input distribution, ensuring unbiased estimates of the output quantities. The input-output data set is sometimes referred to as the experimental design data, since the inputs are following the input distribution, i.e., $\mathbf{x} \sim f_{\mathbf{X}}(\mathbf{x})$. Using the data set, we can obtain approximate DD-GPCE coefficients $\tilde{\mathbf{c}} = (\tilde{c}_1, \dots, \tilde{c}_{L_{N,S,m}})^\top$ by finding the least-squares solution, i.e.,

$$\tilde{\mathbf{c}} = \arg \min_{\mathbf{c} \in \mathbb{R}^{L_{N,S,m}}} \|\mathbf{b} - \mathbf{A}\mathbf{c}\|_2, \quad (21)$$

where

$$\mathbf{A} := \begin{bmatrix} \tilde{\Psi}_1(\mathbf{x}^{(1)}) & \cdots & \tilde{\Psi}_{L_{N,S,m}}(\mathbf{x}^{(1)}) \\ \vdots & \ddots & \vdots \\ \tilde{\Psi}_1(\mathbf{x}^{(L')}) & \cdots & \tilde{\Psi}_{L_{N,S,m}}(\mathbf{x}^{(L')}) \end{bmatrix} \quad \text{and} \quad \mathbf{b} := (y(\mathbf{x}^{(1)}), \dots, y(\mathbf{x}^{(L')}))^\top. \quad (22)$$

From (22), the terms $\tilde{\Psi}_i(\mathbf{x}^{(l)})$ are approximations of $\Psi_i(\mathbf{x}^{(l)})$ resulting from the construction of the monomial moment matrix in Section 2.4.1. According to SLS, the optimal expansion coefficients are

obtained by minimizing the mean-squared residual

$$\hat{e}_{S,m} := \frac{1}{L'} \sum_{l=1}^{L'} \left[y(\mathbf{x}^{(l)}) - \sum_{i=1}^{L_{N,S,m}} \tilde{c}_i \tilde{\Psi}_i(\mathbf{x}^{(l)}) \right]^2. \quad (23)$$

The least-squares solution $\tilde{\mathbf{c}}$ is obtained from the normal equations $\mathbf{A}^\top \mathbf{A} \tilde{\mathbf{c}} = \mathbf{A}^\top \mathbf{b}$, where the $L_{N,S,m} \times L_{N,S,m}$ matrix $\mathbf{A}^\top \mathbf{A}$ is referred to as the information or data matrix. If $\mathbf{A}^\top \mathbf{A}$ is positive-definite then the solution the least-squares approximation of the DD-GPCE coefficients is

$$\tilde{\mathbf{c}} = (\mathbf{A}^\top \mathbf{A})^{-1} \mathbf{A}^\top \mathbf{b}. \quad (24)$$

When using SLS, the number of experimental data must be larger than the number of coefficients, that is, $L' > L_{N,S,m}$. Even if this condition is met, the experimental design must be carefully chosen to ensure that the resulting matrix $\mathbf{A}^\top \mathbf{A}$ is well-conditioned.

In this work, the data \mathbf{A}, \mathbf{b} for the least-squares solution $\tilde{\mathbf{c}}$ in (21) is obtained from MCS. This satisfies the required accuracy of the estimates of the DD-GPCE coefficients in all examples we considered. Alternatively, one may perform several optimal design of experiments which have proven to be effective in the stability of the least-squares solution, see [10, 24].

3. Sampling-based CVaR estimation by dimensionally decomposed GPCE

This section shows how the DD-GPCE can be leveraged for sampling-based CVaR estimation. We include a discussion of the difference in convergence rate when the two—theoretically equivalent—CVaR expressions are used in practice. We finish the section by presenting a complete algorithm. The estimation of VaR in (3) and CVaR in either (5) or (6) for nontrivial examples requires a sampling method, such as MCS, Quasi MCS (QMCS), or Latin hypercube sampling (LHS). We follow the sampling-based MC algorithm from [12, Alg. 2.1].

The S -variate, m th-order DD-GPCE $y_{S,m}(\mathbf{X})$, presented in Section 2.4, can be employed as an inexpensive surrogate model that replaces an expensive-to-evaluate function $y(\mathbf{X})$. Thus, the sampling-based estimation is performed with $y_{S,m}(\mathbf{x})$ and we denote the estimates by $\widehat{\text{VaR}}_\beta[y_{S,m}(\mathbf{X})]$ and $\widehat{\text{CVaR}}_\beta[y_{S,m}(\mathbf{X})]$. Algorithm 1 summarizes all steps of the estimation process.

We employ Algorithm 1 for standard MC sampling, where the probability $p^{(l)} = 1/L$ for $l = 1, \dots, L$. We note that the algorithm can also be used in the context of importance sampling, in which case $p^{(l)} = \omega(\mathbf{x}^{(l)})/M$, $l = 1, \dots, M \ll L$, with $\omega(\cdot)$ being the weight function, see [12].

While the computation of the value at-risk is straightforward (see Steps 3-4 in Algorithm 1), the computation of the CVaR estimate in Step 5 requires further discussion, as outlined next. Based on the two equivalent definitions of $\text{CVaR}_\beta[y(\mathbf{X})]$ in (5) and (6), one can obtain the estimate

$$\widehat{\text{CVaR}}_\beta[y_{S,m}(\mathbf{X})] = \widehat{\text{VaR}}_\beta[y_{S,m}(\mathbf{X})] + \frac{1}{1-\beta} \frac{1}{L} \sum_{l=1}^L \left(y_{S,m}(\mathbf{x}^{(l)}) - \widehat{\text{VaR}}_\beta[y_{S,m}(\mathbf{X})] \right)_+ \quad (25)$$

from (5) or one can compute it from (6) as

$$\widehat{\text{CVaR}}_\beta[y_{S,m}(\mathbf{X})] = \frac{1}{1-\beta} \frac{1}{L} \sum_{l=1}^L y_{S,m}(\mathbf{x}^{(l)}) \mathbb{I}_{\{y_{S,m} \geq \widehat{\text{VaR}}_\beta[y_{S,m}(\mathbf{X})]\}}(y_{S,m}(\mathbf{x}^{(l)})). \quad (26)$$

For the sampling-based estimation employing Algorithm 1, we found that the convergence rate of these two CVaR estimates can be significantly different. The estimate (25) is generally converging faster than the one (26), so we use (25) in this study.

Remark 1. Algorithm 1 produces unbiased estimates for $\text{VaR}_\beta[y(\mathbf{X})]$ and $\text{CVaR}_\beta[y(\mathbf{X})]$ from samples $y(\mathbf{x}^{(l)})$, $l = 1, \dots, L$. For asymptotic convergence properties of the sampling-based estimators $\widehat{\text{VaR}}_\beta[y(\mathbf{X})]$ and $\widehat{\text{CVaR}}_\beta[y(\mathbf{X})]$ c.f. [13, Theorem 2.1]; for instance the estimates have distinct convergence rates, $\mathcal{O}(L^{-3/4}(\log L)^{3/4})$ and $\mathcal{O}(L^{-1} \log L)$, respectively. We note that standard MCS requires L evaluations of the output $y(\mathbf{x}^{(l)})$ for $l = 1, \dots, L$, which can create prohibitive computational demands and one may not have enough resources to obtain converged VaR_β and CVaR_β estimates. In contrast, the MCS with the DD-GPCE approximation requires evaluations of simple polynomial functions to obtain $y_{S,m}$. Taking a large number of samples from the DD-GPCE allows us to obtain converged CVaR solutions.

Moreover, the DD-GPCE approximation $y_{S,m}$ of y converges to y as $S \rightarrow N$ and $m \rightarrow \infty$ in the mean-square sense. As a surrogate model, however, the DD-GPCE usually has a model error, which means that $y_{S,m} \approx y$ (except we get equality when y is a polynomial function and the same degree (S) and order (m) of y are selected for the DD-GPCE) and so, in general, $\widehat{\text{CVaR}}_\beta[y_{S,m}(\mathbf{X})]$ does not converge to $\text{CVaR}_\beta[y(\mathbf{X})]$. Our numerical results in Section 5 show that the bias is minimal.

Algorithm 1 Sampling-based estimation of VaR_β and CVaR_β by the S -variate, m th-order DD-GPCE approximation $y_{S,m}$.

Input: Samples $\mathbf{x}^{(l)} = (x_1^{(l)}, \dots, x_N^{(l)})^\top$, $l = 1, \dots, L \gg 1$, via MCS, QMCS, or LHS with corresponding probabilities $p^{(l)} = f_{\mathbf{X}}(\mathbf{x}^{(l)})d\mathbf{x}^{(l)}$; Set a risk level $\beta \in (0, 1)$.

Output: Estimates $\widehat{\text{VaR}}_\beta[y_{S,m}(\mathbf{X})]$ and $\widehat{\text{CVaR}}_\beta[y_{S,m}(\mathbf{X})]$.

- 1: Create output samples $y_{S,m}(\mathbf{x}^{(l)}) \simeq y(\mathbf{x}^{(l)})$, $l = 1, \dots, L$.
- 2: Sort values of y in descending order and relabel the samples so that

$$y_{S,m}(\mathbf{x}^{(1)}) > y_{S,m}(\mathbf{x}^{(2)}) > \dots > y_{S,m}(\mathbf{x}^{(L)}),$$

and reorder the probabilities accordingly (so that $p^{(l)}$ corresponds to $\mathbf{x}^{(l)}$).

- 3: Compute the index $\tilde{k}_\beta \in \mathbb{N}$ such that

$$\sum_{l=1}^{\tilde{k}_\beta-1} p^{(l)} \leq 1 - \beta < \sum_{l=1}^{\tilde{k}_\beta} p^{(l)}.$$

- 4: Set $\widehat{\text{VaR}}_\beta[y_{S,m}(\mathbf{X})] = y_{S,m}(\mathbf{x}^{(\tilde{k}_\beta)})$.

- 5: Set $\text{CVaR}_\beta[y(\mathbf{X})] \approx \widehat{\text{CVaR}}_\beta[y_{S,m}(\mathbf{X})]$ in (25).
-

The DD-GPCE relies on SLS or its variants, where the output sample size is usually determined as at least three or four times of the number of basis functions or expansion coefficients. Thereby, for risk measures of high-dimensional inputs (say, $N \geq 20$), the DD-GPCE mandates obtaining hundreds of output samples, which can be computationally intensive when that requires expensive high-fidelity model evaluations. For such cases, we propose a novel bi-fidelity method to efficiently compute the DD-GPCE, as introduced in the following section.

4. Bi-fidelity method for CVaR estimation

In practical applications, the output $y(\mathbf{X}) \in L^2(\Omega, \mathcal{F}, \mathbb{P})$ requires the simulation of a computational model, e.g., via FEA. This allows the user to choose the level of fidelity. Computationally expensive high-fidelity models produce accurate solutions whereas faster lower-fidelity models, by definition, introduce output bias (or error). Multifidelity methods combine models with multiple fidelities to solve UQ problems and can produce excellent results with provable guarantees at much lower cost, see the survey [33] and references therein.

This section introduces a novel bi-fidelity method that combines the benefits of lower- and high-fidelity models for the construction of DD-GPCE approximations and their subsequent deployment for precise and efficient CVaR estimation under arbitrary dependent random inputs. We define relations of high and low-fidelity output in Section 4.1, present a novel Fourier polynomial expansion for high-fidelity output in Section 4.2, and describe the complete algorithm of the proposed bi-fidelity method for CVaR estimation and its cost in Section 4.3.

4.1. Relations of high and low-fidelity output

For $y(\mathbf{X}) \in L^2(\Omega, \mathcal{F}, \mathbb{P})$, we denote by $y_H(\mathbf{X})$ and $y_L(\mathbf{X})$ the random output estimated by the high- and low-fidelity models of y , respectively, which are both functions of the same random input $\mathbf{X} \in \mathbb{A}^N \subseteq \mathbb{R}^N$ and thus share the identical sample space Ω . Let $Y_L := y_L(\mathbf{X})$ whose PDF $f_{Y_L}(y_L)$ is on the domain of Y_L , denoted by $\bar{\mathbb{A}} \subseteq \mathbb{R}$.

Consider a function $h : \bar{\mathbb{A}} \rightarrow \mathbb{R}$ of Y_L that approximates the high-fidelity output $y_H(\mathbf{X})$, i.e.,

$$y_H(\mathbf{X}) \approx h(Y_L). \quad (27)$$

The mapping h suggests that the relationship between input and output is much simpler than the high-fidelity model y_H . Thus, we approximate the high-fidelity output via the mapping $h(Y_L)$; we do so with a low-degree Fourier-polynomial expansion with measure-consistent orthonormal polynomials in Y_L , which can be shown to have nearly exponential convergence [37]. The Fourier-polynomial expansion will be introduced in the following subsection.

4.2. Fourier polynomial expansion to approximate the high-fidelity output

Given a random variable Y_L satisfying Assumption 1, the mapping $h(Y_L)$ in (27) can be obtained via its \bar{m} -th-order Fourier polynomial expansion as

$$h_{\bar{m}}(Y_L) = \sum_{i=1}^{\bar{m}+1} b_i \Psi_i(Y_L), \quad (28)$$

with its expansion coefficients

$$b_i = \int_{\bar{\mathbb{A}}} h(y_L) \Psi_i(y_L) f_{Y_L}(y_L) dy_L, \quad i = 1, \dots, \bar{m} + 1.$$

Here, $\Psi_i(Y_L)$, $i = 1, \dots, \bar{m} + 1$ are orthonormal polynomials that are consistent with the probability measure $f_{Y_L}(y_L) dy_L$ of the low-fidelity output random variable Y_L . These orthogonal polynomials are determined by a three-step process, as described next.

4.2.1. Orthonormal polynomial construction

For $j \in \mathbb{N}_0$ and $y_L \in \bar{\mathbb{A}} \subseteq \mathbb{R}$, a monomial in the real variable y_L is y_L^j and has a degree j . Consider for each $\bar{m} \in \mathbb{N}_0$ the elements of the ordered index set $\{j \in \mathbb{N}_0 : j \leq \bar{m}\}$. The set has cardinality $\bar{m} + 1$. We denote by

$$\Psi_{\bar{m}}(y_L) = (\Psi_1(y_L), \dots, \Psi_{\bar{m}+1}(y_L))^T, \quad (29)$$

the $\bar{m} + 1$ -dimensional vector of orthonormal polynomials that are consistent with the probability measure $f_{Y_L}(y_L) dy_L$ of Y_L . This vector is determined as follows.

Step 1. Given $\bar{m} \in \mathbb{N}_0$, $m \in \mathbb{N}_0$, and $0 \leq S \leq m$, determine an $(\bar{m} + 1)$ -dimensional column vector

$$\mathbf{M}_{\bar{m}}(y_L) = (1, y_L, y_L^2, \dots, y_L^{\bar{m}})^T, \quad (30)$$

of monomials y_L^j for $|j| \leq \bar{m}$. The real variable y_L can be replaced with the S -variate, m th-order DD-GPCE

$$\tilde{y}_{L,S,m}(\mathbf{x}) = \sum_{i=1}^{L_{N,S,m}} \bar{c}_i \Psi_i(\mathbf{x}), \quad (31)$$

where

$$\bar{c}_i = \int_{\mathbb{A}^N} y_L(\mathbf{x}) \Psi_i(\mathbf{x}) f_{\mathbf{X}}(\mathbf{x}) d\mathbf{x}$$

and $\Psi_i(\mathbf{x})$, $i = 1, \dots, L_{N,S,m}$, are orthonormal polynomials consistent with the probability measure $f_{\mathbf{X}}(\mathbf{x}) d\mathbf{x}$ of \mathbf{X} . Then, the resulting $(\bar{m} + 1)$ -dimensional column vector of $\tilde{\mathbf{M}}_{\bar{m}}(y_L)$ is

$$\tilde{\mathbf{M}}_{\bar{m}}(y_L) = (1, \tilde{y}_{L,S,m}, \dots, \tilde{y}_{L,S,m}^{\bar{m}})^{\top}. \quad (32)$$

Step 2. Construct an $(\bar{m} + 1) \times (\bar{m} + 1)$ monomial moment matrix of $\tilde{\mathbf{M}}_{\bar{m}}(y_L)$, defined as

$$\tilde{\mathbf{G}}_{\bar{m}} := \mathbb{E}[\tilde{\mathbf{M}}_{\bar{m}}(Y_L) \tilde{\mathbf{M}}_{\bar{m}}^{\top}(Y_L)] = \int_{\bar{\mathbb{A}}} \tilde{\mathbf{M}}_{\bar{m}}(y_L) \tilde{\mathbf{M}}_{\bar{m}}^{\top}(y_L) f_{Y_L}(y_L) dy_L. \quad (33)$$

For an arbitrary PDF $f_{Y_L}(y_L)$, $\tilde{\mathbf{G}}_{\bar{m}}$ can be estimated with good accuracy by sampling methods, such as MCS, QMCS, or LHS, etc.

Step 3. Select the $(\bar{m} + 1) \times (\bar{m} + 1)$ whitening matrix $\tilde{\mathbf{W}}_{\bar{m}}$ from the Cholesky decomposition of the monomial moment matrix $\tilde{\mathbf{G}}_{\bar{m}}$ [37], leading to

$$\tilde{\mathbf{W}}_{\bar{m}}^{-1} \tilde{\mathbf{W}}_{\bar{m}}^{-\top} = \tilde{\mathbf{G}}_{\bar{m}}. \quad (34)$$

Then employ the whitening transformation to generate orthonormal polynomials from

$$\tilde{\Psi}_{\bar{m}}(y_L) = \tilde{\mathbf{W}}_{\bar{m}} \tilde{\mathbf{M}}_{\bar{m}}(y_L). \quad (35)$$

These three steps are similar to those used for creating measure-consistent orthonormal polynomials in Section 2.4.1. However, in Steps 1 and 2 of the latter for Y_L , the realizations of Y_L are determined by S -variate, m th-order DD-GPCE approximations. In doing so, the same basis functions $\Psi_i(\mathbf{X})$, $i = 1, \dots, L_{N,S,m}$, created in the three-step process in Section 2.4.1 are reused. Furthermore, their respective DD-GPCE coefficients \bar{c}_i , $i = 1, \dots, L_{N,S,m}$, are computed via SLS using the computationally economical lower-fidelity model. Therefore, the latter three-step process can be performed efficiently. As discussed earlier for the related three-step process in Section 2.4.1, constructing a well-conditioned version of the monomial moment matrix is critical in implementing the Cholesky factorization in (34).

4.2.2. Expansion coefficients

For $h : \bar{\mathbb{A}} \rightarrow \mathbb{R}$ and a realization $\mathbf{x} = (x_1, \dots, x_N) \in \mathbb{A}^N$ of \mathbf{X} , let the input-output data set be

$$\{y_L^{(l)}, y_H^{(l)}\}_{l=1}^{L''} := \{y_L(\mathbf{x}^{(l)}), y_H(\mathbf{x}^{(l)})\}_{l=1}^{L''},$$

with sample size $L'' \in \mathbb{N}$. Then, the coefficients of the Fourier polynomial expansion in (28) are obtained by minimizing the mean-squared residual

$$e''_{S,m} := \frac{1}{L''} \sum_{l=1}^{L''} \left[y_H^{(l)} - \sum_{i=1}^{\bar{m}+1} b_i \Psi_i(y_L^{(l)}) \right]^2 \quad (36)$$

via SLS explained in Section 2.4.3.

Remark 2. *The Fourier-polynomial expansion in (36) includes scalar realizations $y_L^{(l)}$ of the random variable Y_L . The degree \bar{m} is usually set as a small number, say $\bar{m} = 1-3$. Thereby, the requisite sample size L'' , usually determined ad hoc by requiring that $3 \leq L''/(\bar{m} + 1) \leq 8$, is small as well. This makes the bi-fidelity method to approximate the high-fidelity output data using \bar{m} th-order Fourier polynomial expansion computationally economical.*

4.3. Complete algorithm and cost for CVaR estimation

Algorithm 2 presents a complete algorithm for the bi-fidelity method to estimate VaR_β and CVaR_β . The cost to determine the S -variate, m th-order DD-GPCE approximation is dominated by the cost of evaluating the input-output data set $\{\mathbf{x}^{(l)}, y_H(\mathbf{x}^{(l)})\}_{l=1}^{L'}$ which requires $L' \in \mathbb{N}$ high-fidelity model evaluations. In this regard, for high-dimensional problems, the DD-GPCE method via SLS alleviates the curse of dimensionality due to the sample size L' being determined as a multiple of the number of basis functions $L_{N,S,m}$ in (12) instead of the sample size of regular GPCE, $L_{N,m}$, in (7). Additionally, the proposed bi-fidelity method uses low-fidelity models to generate output data that approximate the high-fidelity model well, yielding an overall efficient method to compute the S -variate, m th-order DD-GPCE.

To select the fidelity for both models, the high-fidelity model is usually determined by a convergence test. A strategy for the selection of the low-fidelity models can be devised based on computational cost while maintaining physicality of the solution. Let c_T be the total computational budget and c_H, c_L be the costs of the high-fidelity and low-fidelity model evaluations, respectively. Since the low and high-fidelity output sample sizes L' and L'' are assumed to be inputs in Algorithm 2, the level of the low-fidelity model can be determined by considering its permissible cost c'_L , i.e.,

$$c'_L \leq c_L = \frac{c_T - L''c_H}{L'}$$

Other strategies for selecting the low-fidelity model are discussed in Section 5.2.

5. Numerical results

Two numerical examples are presented to illustrate the proposed DD-GPCE and bi-fidelity methods for estimating CVaR. In Section 5.1, a three-dimensional 36-bar truss structure is considered, followed by an example of a glass/vinylester composite plate in Section 5.2.

In Examples 1 and 2, the sample size L for sampling-based CVaR estimations is 10,000. This number is determined by a convergence test that yielded less than 0.1% difference between the previous and current steps in MCS solutions for both examples. The monomial moment matrices $\mathbf{G}_{S,m}$ and $\mathbf{G}_{\bar{m}}$ in (14) and (33), respectively, are determined by QMCS with $\bar{L} = 5 \times 10^6$ samples together with the Sobol sequence [44]. The selection of the Sobol sequence in this work is due to its simplicity and efficiency in generating low-discrepancy quasi-random samples, thus improving the performance of QMCS.

In both examples, the coefficients of DD-GPCE or regular GPCE are estimated by SLS, c.f. Section 2.4.3. For a satisfactory estimation of the coefficients, we select the factors $L'/L_{N,S,m}$ (in DD-GPCE) or $L'/L_{N,m}$ (in regular GPCE) equal to three and four in Examples 1 and 2, respectively. In Example 2, we determine the number L'' of high-fidelity FEA by selecting the factor $L''/(\bar{m} + 1)$ as eight. The numerical results are obtained using MATLAB [26] on an Intel Core i7-10850H 2.70 GHz processor with 64 GB of RAM.

The CVaR estimates via the S -variate, m th-order DD-GPCE of $y(\mathbf{X})$ are denoted $\widehat{\text{CVaR}}_\beta[y_{S,m}(\mathbf{X})]$. The proposed CVaR solutions are compared with a reference one by crude MCS of the chosen L high-fidelity output data in a single trial.

Algorithm 2 Bi-fidelity method for VaR_β and CVaR_β estimation

Input: Set a risk level $\beta \in (0, 1)$. Set truncation parameters S , m , and \bar{m} . Set sample sizes L , \bar{L} , L' , and L'' . Generate input samples $\{\mathbf{x}^{(l)}\}_{l=1}^L$ from the known probability measure $f_{\mathbf{X}}(\mathbf{x})d\mathbf{x}$ via MCS, QMCS, or LHS.

Output: Estimate $\text{VaR}_\beta[y(\mathbf{X})]$ and $\text{CVaR}_\beta[y(\mathbf{X})]$ in the following steps:

- 1: **procedure** DERIVE ORTHONORMAL (ON) POLYNOMIALS($\Psi_{S,m}(\mathbf{x})$)
 - 2: Set monomial vector $\mathbf{M}_{S,m}(\mathbf{x})$ (13).
 - 3: Create monomial moment matrix $\mathbf{G}_{S,m}$ (14).
 - 4: Create ON polynomial vector $\Psi_{S,m}(\mathbf{x})$ by whitening transformation (15).
 - 5: **end procedure**
 - 6: **procedure** OBTAIN COEFFICIENTS(\bar{c}_i)
 - 7: Generate input-output data set $\{\mathbf{x}^{(l)}, y_L(\mathbf{x}^{(l)})\}_{l=1}^{L'}$ of size $L' \in \mathbb{N}$, where $y_L(\mathbf{x})$ presents a low-fidelity output.
 - 8: Use SLS to estimate \bar{c}_i , $i = 1, \dots, L_{N,S,m}$.
 - 9: **end procedure**
 - 10: Construct the S -variate, m th-order DD-GPCE $\tilde{y}_{L,S,m}(\mathbf{x})$ of low-fidelity output $y_L(\mathbf{x})$ (31).
 - 11: **procedure** DERIVE ON POLYNOMIALS($\Psi_{\bar{m}}(y_L)$)
 - 12: Set monomial vector $\tilde{\mathbf{M}}_{\bar{m}}(y_L)$ via $\tilde{y}_{L,S,m}$ (32).
 - 13: Construct monomial moment matrix $\tilde{\mathbf{G}}_{\bar{m}}$ (33).
 - 14: Create ON polynomial vector $\tilde{\Psi}_{\bar{m}}(y_L)$ by whitening transformation (34).
 - 15: **end procedure**
 - 16: **procedure** OBTAIN COEFFICIENTS(b_i)
 - 17: Generate input-output data set $\{y_L^{(l)}, y_H^{(l)}\}_{l=1}^{L''}$ of size $L'' \in \mathbb{N}$
 - 18: Use SLS to estimate b_i , $i = 1, \dots, \bar{m} + 1$.
 - 19: **end procedure**
 - 20: Construct the \bar{m} th-order Fourier polynomial expansion $y_{H,\bar{m}}(\mathbf{x})$ of high-fidelity output $y_H(\mathbf{x})$ (28).
 - 21: By replacing y with $y_{H,\bar{m}}$, construct $y_{S,m}$ (19) and then perform Algorithm 1 to estimate VaR_β and CVaR_β .
-

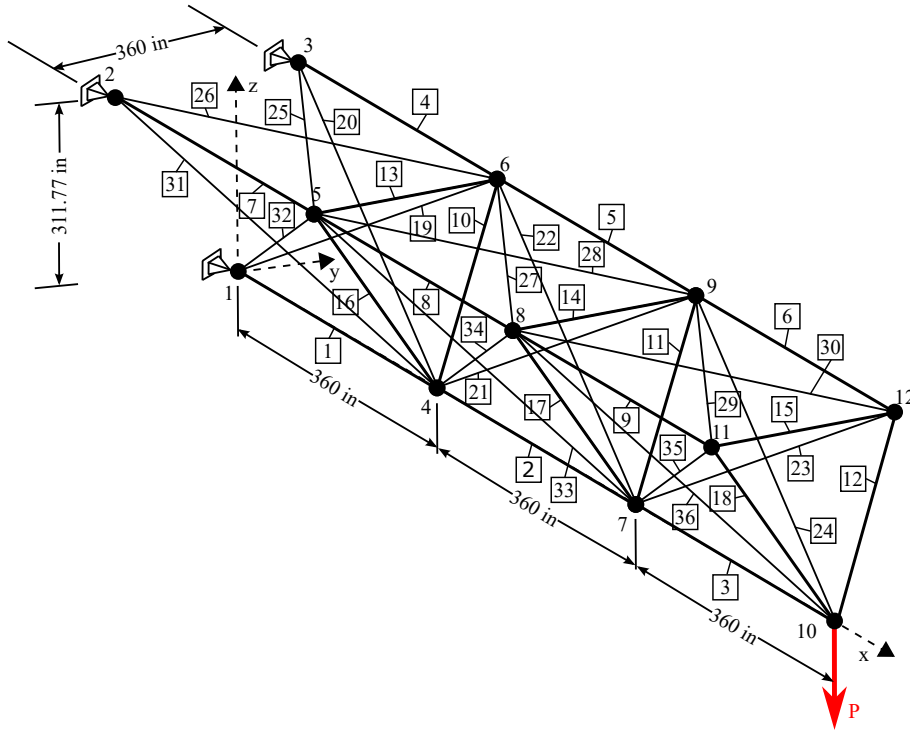


Figure 1: Geometry, loading, and boundary conditions of the 36-bar 3D truss.

To measure the deviation of the proposed CVaR solution from that crude MCS estimate, we provide the mean relative difference (MRD) with respect to the crude MCS $\widehat{\text{CVaR}}_{\beta}[y(\mathbf{X})]$, i.e.,

$$\text{MRD} = \frac{\frac{1}{K} \sum_{k=1}^K \left| \widehat{\text{CVaR}}_{\beta}[y(\mathbf{X})] - \widehat{\text{CVaR}}_{\beta}[y_{S,m}^{(k)}(\mathbf{X})] \right|}{\left| \widehat{\text{CVaR}}_{\beta}[y(\mathbf{X})] \right|}, \quad (37)$$

where $\widehat{\text{CVaR}}_{\beta}[y_{S,m}^{(k)}(\mathbf{X})]$ is the estimate obtained on the k th trial, and K (the number of trials) is 20 in both Examples 1 and 2. At each trial, whether employing either the DD-GPCE, the regular GPCE, or Fourier-polynomial approximation for calculating DD-GPCE, we randomly select a subset of the 10,000 high-fidelity output samples that are already available from the crude MCS. The MRD presents only the mean deviation of a set of proposed CVaR solutions over K trials from a benchmark one obtained by crude MCS, which is not exact but approximate. We also report the average CVaR estimates over 20 trials on Tables 1 and 3 in Examples 1 and 2, respectively.

5.1. Example 1: A 36-bar 3D truss structure

This example demonstrates the efficacy of the DD-GPCE method in estimating the conditional value-at-risk of a system with a relatively high number ($N = 36$) of dependent input random variables.

5.1.1. Problem description

Figure 1 shows a 36-bar three dimensional truss that is simply supported at nodes 1, 2, and 3 and that is subject to a vertically downward concentrated force of 100 lb at node 10. The truss is made of an aluminium alloy characterized by a Young's modulus of 10^7 psi and a mass density of 0.1 lb/in^3 .

Table 1: CVaR_β estimates of two different output functions y_1 and y_2 of the 36-bar 3D truss structure via DD-GPCE and regular GPCE approximations and crude MCS in two distinct cases: Case 1 ($\beta = 0.95$) and Case 2 ($\beta = 0.99$): The sampling-based solutions $\widehat{\text{CVaR}}_\beta$ are computed with a total of $L = 10,000$ samples.

Method	Max. abs. displacement (in)		Max. abs. axial stress (psi)		Number of FEA for each trial
	$\widehat{\text{CVaR}}_\beta$	MRD in (37)	CVaR_β	MRD in (37)	
Case 1 ($\beta = 0.95$)					
1st-order regular GPCE ^(a)	7.2102 ^(b)	2.9533×10^{-2}	14010.1129 ^(b)	3.8101×10^{-2}	111
Univariate, 2nd-order DD-GPCE ^(c)	7.2425 ^(b)	2.5188×10^{-2}	14183.8278 ^(b)	2.6174×10^{-2}	219
Univariate, 3rd-order DD-GPCE ^(d)	7.2439 ^(b)	2.4992×10^{-2}	14240.7163 ^(b)	2.2269×10^{-2}	327
2nd-order regular GPCE ^(e)	7.2435 ^(b)	2.5049×10^{-2}	14153.3969 ^(b)	2.8264×10^{-2}	2,109
crude MCS	7.2448 ^(f)	–	14157.2911 ^(f)	–	10,000
Case 2 ($\beta = 0.99$)					
1st-order regular GPCE ^(a)	7.3642 ^(b)	8.7960×10^{-3}	14313.9756 ^(b)	1.7239×10^{-2}	111
Univariate, 2nd-order DD-GPCE ^(c)	7.4233 ^(b)	8.5367×10^{-4}	14633.5749 ^(b)	6.2756×10^{-3}	219
Univariate, 3rd-order DD-GPCE ^(d)	7.4276 ^(b)	2.7018×10^{-4}	14769.4983 ^(b)	1.4554×10^{-2}	327
2nd-order regular GPCE ^(e)	7.4251 ^(b)	6.0558×10^{-4}	14582.7015 ^(b)	1.3539×10^{-3}	2,109
crude MCS	7.4296 ^(f)	–	14565.0584 ^(f)	–	10,000

- a. The first-order ($m = 1$) regular GPCE is the same as the univariate ($S = 1$), first-order ($m = 1$) DD-GPCE.
b. The CVaR estimate is averaged over 20 trials.
c. The truncation parameters are $S = 1$ and $m = 2$.
d. The truncation parameters are $S = 1$ and $m = 3$.
e. The second-order ($m = 2$) regular GPCE is the same as the bivariate ($S = 2$), second-order ($m = 2$) DD-GPCE.
f. The CVaR estimate is computed by crude MCS in one trial.

There are $N = 36$ random variables $\mathbf{X} = (X_1, \dots, X_{36})^\top$ representing the respective random cross-sectional areas of thirty-six bars, that is, X_i is the i th cross-sectional area, for $i = 1, \dots, 36$. Described as multivariate Gaussian random variables, they have means $\mathbb{E}[X_i] = 30$ and standard deviations equal to $0.05 \mathbb{E}[X_i]$, $i = 1, \dots, 36$; and correlation coefficients $\rho_{ij} = 0.5$, $i, j = 1, \dots, 36$, $i \neq j$. The problem is to determine $\text{VaR}_\beta[y_l(\mathbf{X})]$ and $\text{CVaR}_\beta[y_l(\mathbf{X})]$, $l = 1, 2$, for two different quantile levels: $\beta = 0.95$ (Case 1) and $\beta = 0.99$ (Case 2). We consider two separate output quantities of interest, namely

$$y_1(\mathbf{X}) = \max\{|u_1(\mathbf{X})|, \dots, |u_{12}(\mathbf{X})|, |v_1(\mathbf{X})|, \dots, |v_{12}(\mathbf{X})|\}, \quad (38)$$

$$y_2(\mathbf{X}) = \max\{|\sigma_1(\mathbf{X})|, \dots, |\sigma_{36}(\mathbf{X})|\}. \quad (39)$$

Here, $|u_i|$ and $|v_i|$, are the absolute values of horizontal and vertical displacements, respectively, at the i th nodal point for $i = 1-12$ and $|\sigma_i|$ is the absolute of axial stress of the i th bar for $i = 1-36$. These quantities are determined via the spatially three-dimensional FEA for the linear elastic truss structure, which is implemented in Matlab with truss elements. The two cases of β are shown to demonstrate the robustness of the DD-GPCE method for CVaR estimation with different risk levels.

5.1.2. Results

Table 1 summarizes the sampling-based solution $\widehat{\text{CVaR}}$ of $y_1(\mathbf{X})$ and $y_2(\mathbf{X})$ in Cases 1 and 2, including the requisite numbers of FEA by the regular GPCE and DD-GPCE methods. For comparison between the two methods, we also provide benchmark solutions in the form of crude MCS with 10,000 FEA as tabulated in the eighth and first rows from the bottom in Table 1 in Cases 1 and 2, respectively. The regular DD-GPCE and univariate DD-GPCE methods presented in Table 1 yield estimates of CVaR of y_1 and y_2 that are very close to the crude MCS. Indeed, the range of their maximum value

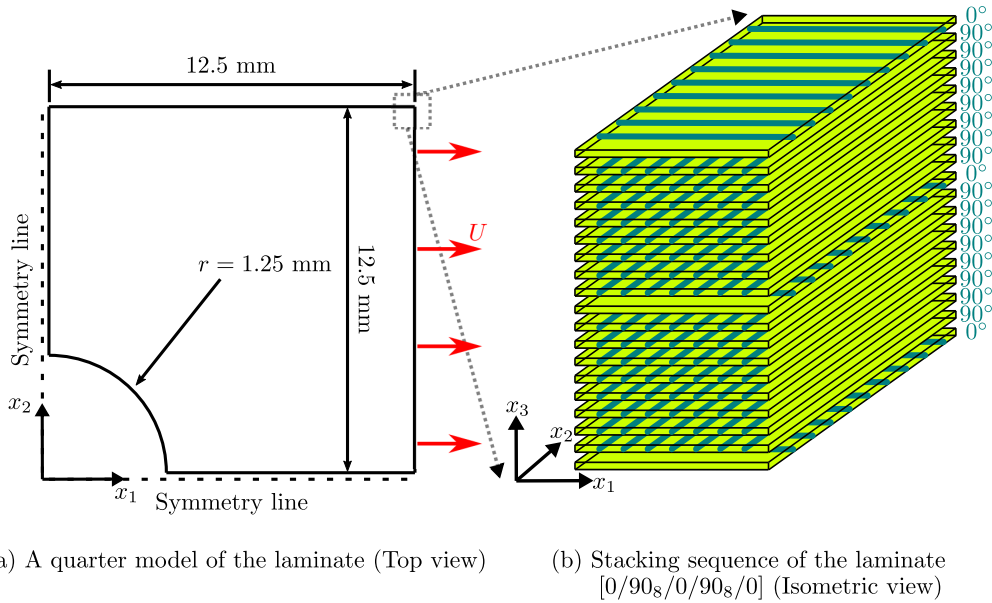


Figure 2: Geometry, loading, and boundary conditions of a glass/vinylester composite plate: We consider one quarter of the full plate domain, which can represent the original square plate with domain $\mathcal{D} = (25 \text{ mm} \times 25 \text{ mm})$ including a circular hole of radius $r = 1.25 \text{ mm}$ in the center due to the symmetry conditions in the x_1 and x_2 directions of the center lines.

of MRD over 20 trials is from 2.95% to 3.81% for the outputs of interest y_1 and y_2 for two cases of β . As expected, the first-order ($m = 1$) regular GPCE approximations of y_1 and y_2 in both Cases 1 and 2 all show relatively lower precision than the other methods. Observe that employing a second-order ($m = 2$) regular GPCE approximation results in more precise CVaR estimates but the required FEA evaluations increase exponentially from 111 ($m = 1$) to 2,109 ($m = 2$). Therefore, for this high-dimensional ($N = 36$) problem, the regular GPCE's curse of dimensionality becomes apparent. On the other hand, the univariate ($S = 1$) DD-GPCE approximations demand only 219–327 FEA evaluations as the degree m increases from two to three; meanwhile, the accuracy of these solutions is better than those of the first-order ($m = 1$) regular GPCE approximations. In particular, for y_1 , the CVaR solutions by all univariate ($S = 1$) DD-GPCE's are almost identical to those by the second-order ($m = 2$) regular GPCE, but the DD-GPCE-based solutions provide a 5–10 \times cost savings compared to the second-order ($m = 2$) regular GPCE. This illustrates the benefits of the proposed DD-GPCE method over the regular GPCE method in terms of computational efficiency for CVaR estimation with relatively high-dimensional dependent random input variables.

5.2. Example 2: A glass/vinylester composite plate

The second example focuses on an additional computational challenge, namely a nonlinear quasi-static FEA with a high number of internal states, where surrogate modeling is required to make the problem tractable. Therefore, the proposed bi-fidelity method from Section 4 is demonstrated. The number of dependent input random variables is moderate to high at $N = 28$.

5.2.1. Problem description

Consider a two-dimensional square plate with spatial domain $\mathcal{D} = (25 \text{ mm} \times 25 \text{ mm})$, including a circular hole of radius $r = 1.25 \text{ mm}$ in the center. Due to symmetry, we consider only a quarter of the plate, resulting in the domain $\bar{\mathcal{D}} = (12.5 \text{ mm} \times 12.5 \text{ mm})$, as shown in Figure 2a. Figure 2b shows that the glass/vinylester laminate (Fiberite/HyE 9082Af) is composed of 19 stacking sequences

Table 2: Statistical properties of constituents in Fiberite/HyE 9082Af

Random variable	Property	Mean	COV (%)	Lower boundary	Upper boundary	Probability distribution
X_1	E_1 (MPa)	44,700	11.55	35760	53640	Uniform
X_2	E_2 (MPa)	12,700	11.55	10,160	15,240	Uniform
X_3	ν_{12}	0.297	11.55	0.238	0.356	Uniform
X_4	G_{12} (MPa)	5,800	11.55	4,640	6,960	Uniform
X_5	S_{t1} (MPa)	1,020	11.55	816	1,224	Uniform
X_6	S_{t2} (MPa)	40	11.55	32	48	Uniform
X_7	S_{c1} (MPa)	620	11.55	496	744	Uniform
X_8	S_{c2} (MPa)	140	11.55	126	168	Uniform
X_9	$S_{s12}^{(b)}$ (MPa)	60	11.55	48	72	Uniform
$X_{10}-X_{28}^{(a)}$	Plies 1–19 thicknesses	0.144	6	0	∞	Multivariate Lognormal

a. Correlation coefficients among $X_{10}-X_{28}$ are 0.5.

b. $S_{s12} = S_{s23}$.

[0/90₈/0/90₈/0], where ‘0’ indicates a ply having fibers in x_1 direction and 90₈ indicates that eight plies have fibers in x_2 direction. The plate is subjected to a uniaxial tensile displacement loading U that acts on the entire right side edge. The geometry of the composite plate was initially studied by [27].

The local directions are x_1 , x_2 , and x_3 and we define E_i , ν_{ij} , and G_{ij} to be Young’s modulus, Poisson’s ratio, and shear modulus of the plies in the corresponding local directions for $i, j = 1, 2, 3$. Also, let S_{ti} , S_{ci} , and S_{sij} be tensile, compressive, and shear strengths of the plies. The measured material properties and ply thicknesses of the laminate vary, and we therefore model them as $N = 28$ random variables, as presented in Table 2. The 19 random variables that model the ply thickness are modeled as correlated via a multivariate lognormal distribution with a correlation coefficient of 0.5. The remaining 9 random variables are modeled as independent and distributed uniformly.

5.2.2. Hashin damage criterion

To perform a quasi-static damage analysis of the fiber-reinforced composite laminate we choose the Hashin damage model. This captures the nonlinear behavior of the composite material during failure progression, which in turn allows for a detailed description of the failure mechanisms. The damage model includes a damage initiation criterion that takes into account four possible failure modes [7]: (1) fiber breakage in tension (F_f^t), (2) fiber buckling in compression (F_f^c), (3) matrix cracking in tension (F_m^t), and (4) matrix crushing in compression (F_m^c). A fiber-reinforced composite is considered damaged if

$$F_f^t = \left(\frac{\sigma_{11}}{S_{t1}} \right)^2 + \alpha \left(\frac{\sigma_{12}}{S_{s12}} \right)^2 \geq 1.0 \text{ and } \sigma_{11} \geq 0, \quad (40)$$

$$F_f^c = \left(\frac{\sigma_{11}}{S_{c1}} \right)^2 \geq 1.0 \text{ and } \sigma_{11} < 0, \quad (41)$$

$$F_f^t = \left(\frac{\sigma_{22}}{S_{t2}} \right)^2 + \left(\frac{\sigma_{12}}{S_{s12}} \right)^2 \geq 1.0 \text{ and } \sigma_{22} \geq 0, \quad (42)$$

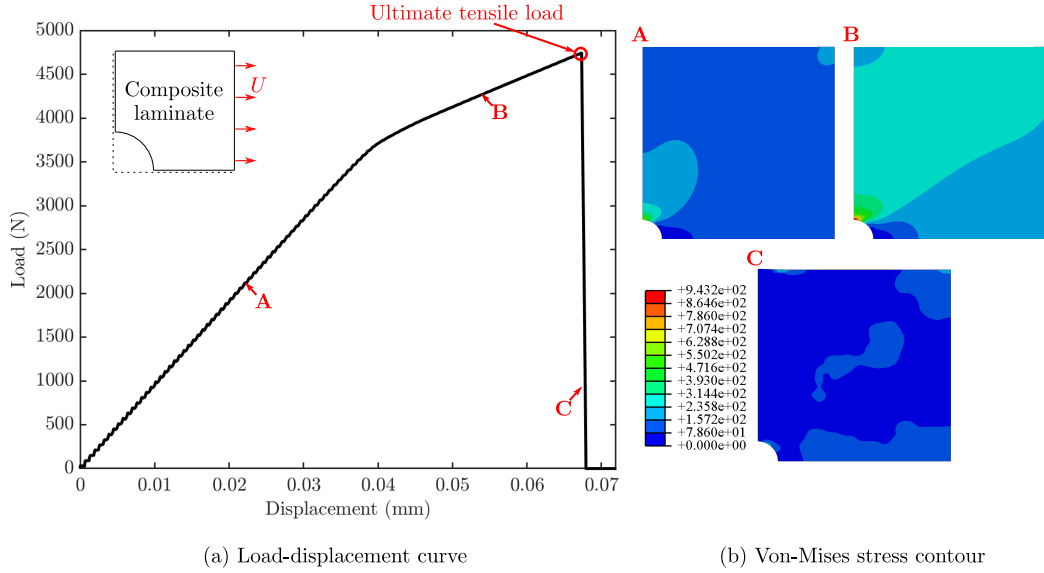


Figure 3: FEA results for the glass/vinylester composite plate: The ultimate tensile load in the load-displacement curve (a) is recorded as the output of interest. Part (b) shows von-Mises stress contour obtained in regimes A, B, and C of the load displacement curve, indicating that the stress concentration occurred at the top of circular hole advances in the regime A to B before a fracture occurs in the regime C.

and

$$F_m^c = \left(\frac{\sigma_{22}}{2S_{s23}} \right)^2 + \left[\left(\frac{S_{c2}}{2S_{s23}} \right)^2 - 1 \right] \frac{\sigma_{22}}{S_{c2}} + \left(\frac{\sigma_{12}}{S_{s12}} \right)^2 \geq 1.0 \text{ and } \sigma_{22} \geq 0, \quad (43)$$

where σ_{11} and σ_{22} are the principal stresses in the x_1 and x_2 directions, respectively, and σ_{12} is the shear stress in x_1 - x_2 plane. Also, the coefficient $\alpha \in [0, 1]$ in (40) accounts for the contribution of the shear stress σ_{12} to the fiber breakage, and set as $\alpha = 1$ in this work. We employ the Hashin criterion together with the progressive damage model; both are built-in functions in ABAQUS/Explicit, version 6.14-2.

5.2.3. Output of interest

The ultimate tensile load is chosen as the output quantity of interest. Figure 3 describes the resulting load versus applied displacement curve of the composite laminate. As the applied displacement at the right edge increases in the range of 0–0.04 mm, the resulting load almost linearly increases, which we label as regime ‘A’ in the figure. However, after the displacement reaches 0.04 mm, the rate of change of the resulting load over the displacement decreases, which we indicate as regime ‘B’ in the figure. This is because the matrix or fiber starts to be degraded as a part of them exceeds the Hashin damage criteria. Thereafter, it reaches a peak value until it drops dramatically. This indicates complete fracture, labeled as regime ‘C’. Indeed, Figure 3b supports the above description of the damage at three marks in Figure 3a. In regime A, the stress concentration appears at the top of the hole, and the stress is further advanced in regime B. Finally, complete damage occurs, fracturing the composite laminate in the x_2 direction from the top of the circular hole and losing the stress distribution at C, as shown in Figure 3b.

Additionally, to confirm the accuracy of the Hashin damage model, we compare the ultimate tensile load (130.45 MPa) by the numerical model for the T300/1034-C laminate with stacking sequence $[0/\pm 40/90_7/90_7/\mp 40/0]$ with experimental results (134.5 MPa) reported in the literature [46]. The

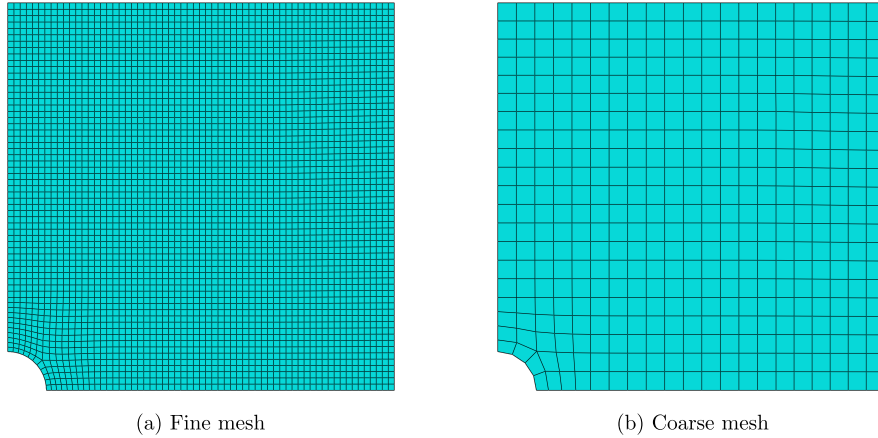


Figure 4: The finite element mesh of the glass/vinylester composite plate: The fine mesh in (a) comprising 3,887 elements is used to generate high-fidelity output data, while the coarse mesh in (b) comprising 441 elements is used to generate lower-fidelity output data.

relative error between experiment and simulation is only 3%.

5.2.4. High-fidelity and low-fidelity models

To evaluate the bi-fidelity method presented in Section 4, the high and low-fidelity outputs were obtained by FEA as follows: the high-fidelity output is computed from a fine mesh model with 3,887 elements, and the lower-fidelity model from a coarse mesh with only 441 elements, as presented in Figures 4a and b, respectively. The element types were chosen as S4R, a 4-node, quadrilateral, stress/displacement shell element with reduced integration, built in ABAQUS/Explicit, version 6.14-2. Therefore, the total number of degrees of freedom for the high-fidelity and lower-fidelity models are 24,084 and 2,910, respectively. The global mesh size (0.2 mm) of the high-fidelity model was determined on the basis of a convergence study, i.e., refining the mesh size globally until the output quantity of interest becomes converged. On the other hand, we determined the low-fidelity model by selecting a larger global mesh size (0.6 mm), where the selected low-fidelity model must be able to capture an ultimate tensile load induced by damage (see Figure 3) at given loading and boundary conditions. Alternatively, the coarse mesh size could be determined in a way that satisfies a given computational budget c_T (4.3), while still maintaining that the solution is physical and realistic. Optimal load management in the spirit of [32] for the surrogate model may also be adapted to CVaR computations.

5.2.5. Results

Table 3 summarizes the CVaR estimates obtained from univariate ($S = 1$) third-order ($m = 3$) DD-GPCE and second-order ($m = 2$) regular GPCE (which is equivalent to the bivariate ($S = 2$) second-order ($m = 2$) DD-GPCE) approximations. Each DD-GPCE, as its three distinct versions, uses (i) the high-fidelity model, (ii) the lower-fidelity model and (iii) the bi-fidelity approximation based on Fourier-polynomial expansions, as presented in Section 4.2. Compared to the standard MCS with 10,000 high-fidelity model evaluations (first row from the bottom of Table 3) the univariate ($S = 1$) DD-GPCE-based CVaR estimates using the high-fidelity model yield 0.743% in MRD. Notably, through proper pruning of basis functions, the univariate ($S = 1$) DD-GPCE-based CVaR estimate requires only 340 FEA (high-fidelity) solutions, leading to a speedup of $29.4\times$ compared to the 859.8 hours of CPU time required for the standard MCS. However, even that CPU time of 29.2 hours for the univariate ($S = 1$) DD-GPCE-based CVaR estimate via the high-fidelity model can still be computationally expensive when users want rapid turnaround in the design processes or when

Table 3: CVaR $_{\beta}$ estimates ($\beta = 0.99$) of the ultimate tensile load of the glass/vinylester composite plate via DD-GPCE approximations and the crude MCS: The sampling-based solutions $\widehat{\text{CVaR}}_{\beta}$ are computed with a total of $L = 10,000$ samples.

Methods	Ultimate tensile load (N)		Number of FEA in a single trial		CPU time in a single trial (hours) ^(c)
	$\widehat{\text{CVaR}}_{\beta}$	MRD in (37)	High-fidelity ^(a)	Low-fidelity ^(b)	
Univariate ($S = 1$), third-order ($m = 3$) DD-GPCE					
High-fidelity output	5540.6511 ^(d)	7.4339×10^{-3}	340	–	29.3
Low-fidelity output	6141.2138 ^(d)	1.0015×10^{-1}	–	340	6.8
Bi-fidelity approximation					
First-order ($\bar{m} = 1$) Fourier-polynomial expansion	5437.7325 ^(d)	2.7375×10^{-2}	16	340	8.1
Second-order ($\bar{m} = 2$) Fourier-polynomial expansion	5451.5180 ^(d)	2.9232×10^{-2}	24	340	8.8
Third-order ($\bar{m} = 3$) Fourier-polynomial expansion	5488.0055 ^(d)	2.1806×10^{-2}	32	340	9.5
Second-order ($m = 2$) regular GPCE (equivalent to bivariate ($S = 2$), second-order ($m = 2$) DD-GPCE)					
High-fidelity output	5576.9167 ^(d)	9.5682×10^{-4}	1,740	–	151.6
Low-fidelity output	6157.3941 ^(d)	1.0305×10^{-1}	–	1,740	36.1
Bi-fidelity approximation					
First-order ($\bar{m} = 1$) Fourier-polynomial expansion	5463.5153 ^(d)	2.7798×10^{-2}	16	1,740	37.5
Second-order ($\bar{m} = 2$) Fourier-polynomial expansion	5442.6036 ^(d)	3.7529×10^{-2}	24	1,740	38.2
Third-order ($\bar{m} = 3$) Fourier-polynomial expansion	5472.6904 ^(d)	2.7351×10^{-2}	32	1,740	38.9
crude MCS	5582.1484 ^(e)	–	10,000	–	859.8

- a. The high-fidelity output is obtained by the fine mesh model in Figure 4a.
- b. The lower-fidelity output is obtained by the coarse mesh model in Figure 4b.
- c. The CPU time is the sum of the CPU time spent executing Algorithm 2 including the number of FEA \times FEA computation time in a single trial. The FEA computation time is averaged over five simulations.
- d. The CVaR estimate is averaged over $K = 20$ trials.
- e. The CVaR estimate is computed by crude MCS in one trial.

used for optimization problems. We also report the univariate ($S = 1$) DD-GPCE solution when only the lower-fidelity model is used. This requires a CPU time of 6.8 hours, almost one-fifth of those 29.3 hours required by the high-fidelity output but yields 10.015% in MRD. Thus, the univariate ($S = 1$) DD-GPCE employing only the lower-fidelity output model yields an inaccurate or biased CVaR estimate, so it is of limited use.

To achieve *almost* the accuracy of the high-fidelity CVaR solution but with the efficiency of the lower-fidelity version, we proposed and tested the proposed bi-fidelity method based on Fourier-polynomial expansion. Indeed, as reported in the eleventh through thirteenth rows from the bottom of the Table 3, all CVaR estimates via the bi-fidelity method are very close to the benchmark CVaR estimate via the crude MCS. As the degree (\bar{m}) increases, the precision of the respective CVaR solution increases from 2.738 % to 2.181 % in MRD, but it shows some fluctuation at the case of $\bar{m} = 2$ due to a random sampling effect. The respective average CVaR solution (the eleventh through thirteenth rows from the bottom in the second column of Table 3) monotonically approaches the benchmark value.

Remarkably, a 2.738 % in MRD can be achieved while needing 8.0 hours in CPU time, which is only marginally higher than the 6.7 hours demanded by the low-fidelity version but provides an almost five-fold improvement in accuracy. Moreover, that third-order ($\bar{m} = 3$) bi-fidelity approximation yields the precision of 2.181 % in MRD by requiring only an additional 32 high-fidelity FEA alongside many lower-fidelity evaluations. This situation is typical for multifidelity UQ methods, where the bulk of the computations are done by lower-fidelity approximations, yet a few high-fidelity solutions provide a significant boost of overall accuracy (and other benefits, see [33]). Moreover, the second-order ($m = 2$) regular GPCE (equivalent to the bivariate ($S = 2$) second-order ($m = 2$) DD-GPCE) approximations provide similar results compared to the univariate ($S = 1$) third-order ($m = 3$) version, as presented in the third through eighth rows of Table 3. In other words, while the bivariate ($S = 2$) DD-GPCE-based CVaR estimate using the high-fidelity model is the most accurate, showing 0.096% in MRD,

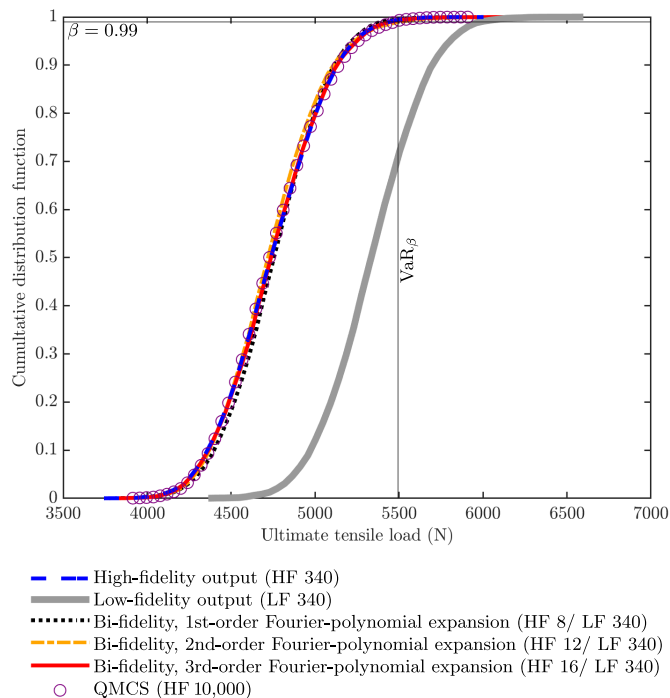


Figure 5: Cumulative distribution function of the ultimate tensile load in the glass/vinylester composite plate: High-fidelity (HF) and low-fidelity (LF) output and three bi-fidelity approximations are used for univariate, 3rd-order DD-GPCE approximations. The calculated DD-GPCE approximations are resampled 10,000 times to estimate the CDFs.

its counterpart using the low-fidelity model yields the lowest accurate solution (10.31% in MRD). However, the requisite number (1,740) of FEA by the bivariate ($S = 2$), second-order ($m = 2$) DD-GPCE is more than five times of those (340) by its univariate ($S = 1$), third-order ($m = 3$) version. As a result, the bivariate DD-GPCE based solution using the high-fidelity model demands almost 151.6 hours in CPU time in each trial which is also more than five times expensive than one (29.3 hours) by the univariate version using the high-fidelity model.

To reduce the 151.6 hours CPU time to the level (36.1 hours) of the low-fidelity version but obtain a more precise CVaR solution than the low-fidelity based solution (10.3% in MRD), we employ the bi-fidelity method. While using first-order ($\bar{m} = 1$) through third-order ($\bar{m} = 3$) approximations of the bi-fidelity method, we obtained more accurate CVaR solutions (2.7% to 3.7% in MRD) than the low-fidelity based solution (10.31% in MRD). Consequently, this result proves that the bi-fidelity method can be effective and robust to the case of bivariate ($S = 2$) DD-GPCE or regular GPCE approximations.

We note that the CPU times (37.5–38.9 hours) by the bivariate ($S = 2$), second-order ($m = 2$) DD-GPCE using the bi-fidelity approximations are higher than those (29.3 hours) by the univariate ($S = 1$), third-order ($m = 3$) DD-GPCE using high-fidelity model. However, the accuracy of the former with bi-fidelity approximations is less than the latter with the high-fidelity model. This result indicates that when a higher value of S or m is chosen than needed to satisfy the user-defined threshold, the efficiency gains diminish for high-dimensional inputs. This is due to rapidly growing number $L_{N,S,m}$ of the coefficients or basis functions as S or m increases. Having said this, the bi-fidelity method improves the accuracy of the CVaR solution significantly (from 10% to 2–3% in MRD) while only requiring slightly more CPU resources (3.9%–7.8%) than the low-fidelity version. These results demonstrate both the robustness of the bi-fidelity method and the power of the DD-GPCE to improve its efficiency by truncating the basis functions in a dimension-wise manner using S . Figure 5 shows

the estimated CDFs of the ultimate tensile load by three distinct versions of the univariate ($S = 1$), third-order ($m = 3$) DD-GPCE approximations, i.e., via high- and low-fidelity output data and also via the bi-fidelity approximation. For each of these distinct methods, a single trial CDF estimate was chosen among the CDF estimates from $K = 20$ trials. For reference, we also show the crude MCS obtained from 10,000 high-fidelity FEA simulations. When the DD-GPCE approximation is computed by the high-fidelity output data of size 340, its CDF is almost identical to the CDF of the crude MCS. On the other hand, the DD-GPCE (of size 340) with only the low-fidelity output produces a CDF that would make an engineer deduce that the composite can withstand much higher tensile loads, which is not true. This can have detrimental effects in engineering practice. In contrast, the proposed DD-GPCE methods in conjunction with the bi-fidelity approximation provide CDF estimates that are very close to those by the crude MCS but require only 16–32 high-fidelity FEA evaluations paired with 340 low-fidelity FEA. Specifically, as the degree \bar{m} of the Fourier-polynomial expansion increases, the respective CDF estimates approach those by the high-fidelity version or the crude MCS very closely. This demonstrates the ability of the proposed bi-fidelity method to accurately estimate CDFs as well.

6. Conclusion and future direction

We presented a novel bi-fidelity method for efficient CVaR estimation of complex nonlinear systems subject to arbitrary and high-dimensional dependent random input variables. The new method entails (1) the DD-GPCE approximation of a stochastic output function with high-dimensional dependent inputs, (2) an innovative method employing Fourier-polynomial expansions of a mapping between the stochastic lower-fidelity and high-fidelity output data for efficiently calculating the DD-GPCE, and (3) a standard sampling-based CVaR estimation integrated with the DD-GPCE. The proposed bi-fidelity method uses measure-consistent orthonormal polynomials in the random variable of the low-fidelity output to approximate the high-fidelity output, thus achieving a nearly exponential convergence rate for the output data. The strength of the bi-fidelity approach is that it only requires a handful of high-fidelity output evaluations to augment the (many) lower-fidelity evaluations. When equipped with high-order (\bar{m}) basis functions, the Fourier-polynomial expansions can achieve more accurate high-fidelity output approximations. The numerical results for the truss structure with $N = 36$ (dependent) random variables showed that CVaR estimation is possible by combining sampling-based CVaR estimation with DD-GPCE approximations. The example demonstrates that DD-GPCE via a dimension-wise reconstruction of the GPCE basis functions can alleviate the curse of dimensionality over the regular GPCE when a high-dimensional problem is addressed. Finally, the power of the proposed bi-fidelity method to achieve nearly the accuracy of the high-fidelity CVaR solution with the efficiency of the low-fidelity version was demonstrated by solving the glass/vinylester laminate problem involving 28 (mostly dependent) input random variables.

The DD-GPCE surrogate can be somewhat limited in terms of accuracy when high-variate interaction effects among input variables are not negligible to the output quantity of interest (i.e., those terms in the PCE cannot be pruned). While the proposed bi-fidelity method uses Fourier-polynomial expansions to approximate the high-fidelity output, it is agnostic to the surrogate model structure. Therefore, in cases where high-variate interactions are relevant, one may need to use and/or develop new surrogate modeling techniques to approximate the output. A potential for improvement of the proposed method is related to the selection of the truncation parameters, e.g., S and m for DD-GPCE or \bar{m} for Fourier-polynomial expansion. Instead of choosing the truncation parameters arbitrarily, one may exploit an adaptive version of DD-GPCE or Fourier-polynomial expansion, where a truncated set of basis is chosen optimally based on a specified error tolerated by the resulting approximation. Moreover, while the bi-fidelity method in this work was mainly used to estimate the value at-risk and the conditional value-at-risk, it can be extended to a more general class of uncertainty quantification problems, such as second-moment or reliability analysis.

Acknowledgment

Funding This material is based on research sponsored by the Air Force Research Lab (AFRL) and Defense Advanced Research Projects Agency (DARPA) under agreement number FA8650-21-2-7126. The U.S. Government is authorized to reproduce and distribute reprints for Governmental purposes notwithstanding any copyright notation thereon.

Disclaimer The views and conclusions contained herein are those of the authors and should not be interpreted as necessarily representing the official policies or endorsements, either expressed or implied, of the AFRL and DARPA or the U.S. Government.

References

- [1] P. Artzner, F. Delbaen, J.-M. Eber, and D. Heath. Coherent measures of risk. *Mathematical finance*, 9(3):203–228, 1999.
- [2] F. Bernal, E. Gobet, and J. Printems. Volatility uncertainty quantification in a stochastic control problem applied to energy. *Methodology and Computing in Applied Probability*, 22(1):135–159, 2020.
- [3] S. L. Brunton, J. Nathan Kutz, K. Manohar, A. Y. Aravkin, K. Morgansen, J. Klemisch, N. Goebel, J. Buttrick, J. Poskin, A. W. Blom-Schieber, T. Hogan, and D. McDonard. Data-driven aerospace engineering: reframing the industry with machine learning. *AIAA Journal*, 59(8):2820–2847, 2021.
- [4] A. Chaudhuri, B. Kramer, M. Norton, J. O. Royset, and K. Willcox. Certifiable risk-based engineering design optimization. *AIAA Journal*, 60(2):551–565, 2022.
- [5] A. Chaudhuri, B. Peherstorfer, and K. Willcox. Multifidelity cross-entropy estimation of conditional value-at-risk for risk-averse design optimization. In *AIAA Scitech 2020 Forum*, page 2129, 2020.
- [6] X. Chen, B. L. Nelson, and K.-K. Kim. Stochastic Kriging for conditional value-at-risk and its sensitivities. In *Proceedings of the 2012 Winter Simulation Conference (WSC)*, pages 1–12. IEEE, 2012.
- [7] A. Duarte, A. D  az S  nchez, and N. Silvestre. Comparative study between XFEM and Hashin damage criterion applied to failure of composites. *Thin-Walled Structures*, 115:277–288, 2017.
- [8] S. Garreis, T. M. Surowiec, and M. Ulbrich. An interior-point approach for solving risk-averse PDE-constrained optimization problems with coherent risk measures. *SIAM Journal on Optimization*, 31(1):1–29, 2021.
- [9] J.-y. Gotoh and S. Uryasev. Support vector machines based on convex risk functions and general norms. *Annals of Operations Research*, 249(1):301–328, 2017.
- [10] M. Hadigol and A. Doostan. Least squares polynomial chaos expansion: A review of sampling strategies. *Computer Methods in Applied Mechanics and Engineering*, 332:382–407, 2018.
- [11] M. Heinkenschloss, B. Kramer, and T. Takhtaganov. Adaptive reduced-order model construction for conditional value-at-risk estimation. *SIAM/ASA Journal on Uncertainty Quantification*, 8(2):668–692, 2020.
- [12] M. Heinkenschloss, B. Kramer, T. Takhtaganov, and K. Willcox. Conditional-value-at-risk estimation via reduced-order models. *SIAM/ASA Journal on Uncertainty Quantification*, 6(4):1395–1423, 2018.

- [13] L. J. Hong, Z. Hu, and G. Liu. Monte Carlo methods for value-at-risk and conditional value-at-risk: a review. *ACM Transactions on Modeling and Computer Simulation (TOMACS)*, 24(4):1–37, 2014.
- [14] J. D. Jakeman, F. Franzelin, A. Narayan, M. Eldred, and D. Pflüger. Polynomial chaos expansions for dependent random variables. *Computer Methods in Applied Mechanics and Engineering*, 351:643–666, 2019.
- [15] J. D. Jakeman, D. P. Kouri, and J. G. Huerta. Surrogate modeling for efficiently, accurately and conservatively estimating measures of risk. *Reliability Engineering & System Safety*, 221:108280, 2022.
- [16] M. C. Kennedy and A. O’Hagan. Predicting the output from a complex computer code when fast approximations are available. *Biometrika*, 87(1):1–13, 2000.
- [17] D. P. Kouri and T. M. Surowiec. Risk-averse PDE-constrained optimization using the conditional value-at-risk. *SIAM Journal on Optimization*, 26(1):365–396, 2016.
- [18] D. P. Kouri and T. M. Surowiec. Epi-regularization of risk measures. *Mathematics of Operations Research*, 45(2):774–795, 2020.
- [19] L. Lattanzi, R. Raffaeli, M. Peruzzini, and M. Pellicciari. Digital twin for smart manufacturing: a review of concepts towards a practical industrial implementation. *International Journal of Computer Integrated Manufacturing*, 34(6):567–597, 2021.
- [20] D. Lee. *Stochastic Optimization for Design Under Uncertainty with Dependent Random Variables*. PhD thesis, The University of Iowa, 2021.
- [21] D. Lee and S. Rahman. Practical uncertainty quantification analysis involving statistically dependent random variables. *Applied Mathematical Modelling*, 84:324–356, 2020.
- [22] D. Lee and S. Rahman. Robust design optimization under dependent random variables by a generalized polynomial chaos expansion. *Structural and Multidisciplinary Optimization*, 63(5):2425–2457, 2021.
- [23] D. Lee and S. Rahman. Reliability-based design optimization under dependent random variables by a generalized polynomial chaos expansion. *Structural and Multidisciplinary Optimization*, 65(1), 2022.
- [24] N. Luthen, S. Marelli, and B. Sudret. Sparse polynomial chaos expansions: Literature survey and benchmark. *SIAM/ASA Journal on Uncertainty Quantification*, 9(2):593–649, 2021.
- [25] R. Mansini, W. Ogryczak, and M. G. Speranza. Conditional value at risk and related linear programming models for portfolio optimization. *Annals of Operations Research*, 152:227–256, 2007.
- [26] MATLAB. *version 9.10.0.1613233 (R2021b)*. The MathWorks Inc., Natick, Massachusetts, 2021.
- [27] M. Moure, S. Sanchez-Saez, E. Barbero, and E. Barbero. Analysis of damage localization in composite laminates using a discrete damage model. *Composites Part B: Engineering*, 66:224–232, 2014.
- [28] M. Navarro, J. A. S. Witteveen, and J. G. Blom. Polynomial chaos expansion for general multivariate distributions with correlated variables. *arXiv preprint arXiv:1406.5483*, 2014.
- [29] S. A. Niederer, M. S. Sacks, M. Girolami, and K. Willcox. Scaling digital twins from the artisanal to the industrial. *Nature Computational Science*, 1(5):313–320, 2021.

- [30] Y. Noh, K. K. Choi, and L. Du. Reliability-based design optimization of problems with correlated input variables using a Gaussian copula. *Structural and Multidisciplinary Optimization*, 38:1–16, 2009.
- [31] M. Norton, V. Khokhlov, and S. Uryasev. Calculating cvar and bpoe for common probability distributions with application to portfolio optimization and density estimation. *Annals of Operations Research*, 299(1):1281–1315, 2021.
- [32] B. Peherstorfer, K. Willcox, and M. Gunzburger. Optimal model management for multifidelity Monte Carlo estimation. *SIAM Journal on Scientific Computing*, 38(5):A3163–A3194, 2016.
- [33] B. Peherstorfer, K. Willcox, and M. Gunzburger. Survey of multifidelity methods in uncertainty propagation, inference, and optimization. *SIAM Review*, 60(3):550–591, 2018.
- [34] N. Pepper, A. Gaymann, S. Sharma, and F. Montomoli. Local bi-fidelity field approximation with knowledge based neural networks for computational fluid dynamics. *Scientific Reports*, 11(1):1–11, 2021.
- [35] H. Rabitz, Ö. Aliş, J. Shorter, and K. Shim. Efficient input-output model representations. *Computer Physics Communications*, 117(1):11–20, 1999.
- [36] S. Rahman. A polynomial dimensional decomposition for stochastic computing. *International Journal for Numerical Methods in Engineering*, 76(13):2091–2116, 2008.
- [37] S. Rahman. A polynomial chaos expansion in dependent random variables. *Journal of Mathematical Analysis and Applications*, 464(1):749–775, 2018.
- [38] S. Rahman. Uncertainty quantification under dependent random variables by a generalized polynomial dimensional decomposition. *Computer Methods in Applied Mechanics and Engineering*, 344:910–937, 2019.
- [39] R. T. Rockafellar and J. O. Royset. Engineering decisions under risk averseness. *ASCE-ASME Journal of Risk and Uncertainty in Engineering Systems, Part A: Civil Engineering*, 1(2):04015003, 2015.
- [40] R. T. Rockafellar and S. Uryasev. Optimization of conditional value-at risk. *Journal of Risk*, 3:21–41, 2000.
- [41] R. T. Rockafellar and S. Uryasev. Conditional value-at-risk for general loss distributions. *Journal of Banking & Finance*, 26(7):1443–1471, 2002.
- [42] J. O. Royset, L. Bonfiglio, G. Vernengo, and S. Brizzolara. Risk-adaptive set-based design and applications to shaping a hydrofoil. *Journal of Mechanical Design*, 139(10):101403, 2017.
- [43] S. Sarykalin, G. Serraino, and S. Uryasev. Value-at-risk vs. conditional value-at-risk in risk management and optimization. In *State-of-the-art decision-making tools in the information-intensive age*, pages 270–294. INFORMS, 2008.
- [44] I. M. Sobol. Distribution of points in a cube and approximate evaluation of integrals. *Zh. Vych. Mat. Mat. Fiz.*, 7:784–802, 1967.
- [45] T. Soma and Y. Yoshida. Statistical learning with conditional value at risk. *arXiv preprint arXiv:2002.05826*, 2020.
- [46] S. C. Tan. A progressive failure model for composite laminates containing openings. *Journal of Composite Materials*, 25(5):556–577, 1991.
- [47] N. Wiener. The homogeneous chaos. *American Journal of Mathematics*, 60(4):897–936, 1938.

- [48] D. Xiu and G. E. Karniadakis. The Wiener-Askey polynomial chaos for stochastic differential equations. *SIAM Journal of Scientific Computing*, 24:619–644, 2002.
- [49] H. Yang and M. Gunzburger. Algorithms and analyses for stochastic optimization for turbofan noise reduction using parallel reduced-order modeling. *Computer Methods in Applied Mechanics and Engineering*, 319:217–239, 2017.
- [50] Z. Zou, D. Kouri, and W. Aquino. An adaptive local reduced basis method for solving PDEs with uncertain inputs and evaluating risk. *Computer Methods in Applied Mechanics and Engineering*, 345:302–322, 2019.

Appendix A. Three step process to construct measure-consistent orthonormal polynomials

This appendix summarizes a process to generate the multivariate orthonormal polynomial basis of GPCE in Section 2.3. The orthonormal polynomial functions are consistent with an arbitrary, non-product-type probability measure $f_{\mathbf{X}}(\mathbf{x})d\mathbf{x}$ of \mathbf{X} and determined by the following three steps.

1. Given $m \in \mathbb{N}_0$, create an $L_{N,m}$ -dimensional column vector

$$\mathbf{M}_m(\mathbf{x}) = (\mathbf{x}^{\mathbf{j}^{(1)}}, \dots, \mathbf{x}^{\mathbf{j}^{(L_{N,m})}})^{\top}, \quad (\text{A.1})$$

of monomials whose elements are the monomials $\mathbf{x}^{\mathbf{j}}$ for $|\mathbf{j}| \leq m$ arranged in the aforementioned order. It is referred to as the monomial vector in $\mathbf{x} = (x_1, \dots, x_N)^{\top}$ of degree at most m .

2. Construct an $L_{N,m} \times L_{N,m}$ monomial moment matrix of $\mathbf{M}_m(\mathbf{X})$, defined as

$$\mathbf{G}_m := \mathbb{E}[\mathbf{M}_m(\mathbf{X})\mathbf{M}_m^{\top}(\mathbf{X})] = \int_{\mathbb{A}^N} \mathbf{M}_m(\mathbf{x})\mathbf{M}_m^{\top}(\mathbf{x})f_{\mathbf{X}}(\mathbf{x})d\mathbf{x}. \quad (\text{A.2})$$

For an arbitrary PDF $f_{\mathbf{X}}(\mathbf{x})$, \mathbf{G}_m cannot be determined exactly, but it can be estimated with good accuracy by numerical integration and/or sampling methods [21].

3. Select the $L_{N,m} \times L_{N,m}$ whitening matrix \mathbf{W}_m from the Cholesky decomposition of the monomial moment matrix \mathbf{G}_m [37], leading to

$$\mathbf{W}_m^{-1}\mathbf{W}_m^{-\top} = \mathbf{G}_m. \quad (\text{A.3})$$

Then employ the whitening transformation to generate multivariate orthonormal polynomials from

$$\mathbf{\Psi}_m(\mathbf{x}) = \mathbf{W}_m\mathbf{M}_m(\mathbf{x}). \quad (\text{A.4})$$